

An ISM-based CNF tracking controller design for uncertain MIMO linear systems with multiple time-delays and external disturbances

Vahid Johari Majd · Saleh Mobayen

Received: 23 June 2014 / Accepted: 1 January 2015 / Published online: 14 January 2015
© Springer Science+Business Media Dordrecht 2015

Abstract In this paper, a combination of integral sliding mode and composite nonlinear feedback method is proposed for fast and accurate robust tracking and model following of uncertain multiple-input multiple-output linear systems with multiple time-delays and external disturbances. The composite nonlinear feedback technique allows following the reference trajectory within a given accuracy and the invariance property of the integral sliding mode method rejects the disturbances and preserves the stability of the closed-loop system. By using the Lyapunov–Krasovskii functional, the conditions for asymptotic stabilization are obtained in the form of linear matrix inequalities. To improve the tracking performance for different reference amplitudes, a new nonlinear function is included in the control law and is optimally tuned using a modified random search algorithm. The selection of sliding surface and the existence of the sliding mode are two significant issues, which have been addressed. This scheme not only guarantees robustness against time-delays and uncertainties, but also avoids chattering phenomenon

and reaching phase. Finally, the simulations are provided to verify the theoretical results. The results show that the proposed method leads to great improvement on the tracking error and the control effort compared to the available methods.

Keywords Integral sliding mode · Composite nonlinear feedback · Time-delays · Robust tracking · Nonlinear function · Uncertain system

1 Introduction

Sliding mode control (SMC) is an important control approach which has been widely used in control engineering to handle linear and nonlinear systems with uncertainties and bounded external disturbances [1–5]. The basic ideas of SMC can be described as follow: First, a switching surface is defined such that the closed-loop system exhibits desired dynamic behavior during sliding mode [6,7]. Second, the sliding mode controller is employed to derive the system states to the sliding surface [8,9]. In the conventional sliding mode control, during the reaching phase, the controlled system is not robust. Moreover, even matched disturbances can destabilize the system [10–12]. For solving this problem, integral sliding mode (ISM) concept has been proposed [13–15]. By adding an integral term to the sliding surface, the reaching phase can be eliminated and the system trajectories start moving on the surface right from the beginning [16,17]. Due to this

V. J. Majd
School of Electrical and Computer Engineering, Tarbiat
Modares University, Tehran, Iran

S. Mobayen (✉)
Department of Electrical Engineering, Faculty of
Engineering, University of Zanjan, P.O. Box 38791-45371,
Zanjan, Iran
e-mail: smobayen@gmail.com; mobayen@znu.ac.ir
URL: http://www.znu.ac.ir/members/mobayen_saleh

capability, ISM has received a lot of attention and it has also been developed for matched and unmatched uncertain systems [18–21]. The main restriction of ISM is that it requires complete knowledge of the states [17].

The composite nonlinear feedback (CNF) control method is developed to improve the transient performance of the closed-loop system by introducing a nonlinear feedback law [22,23]. The CNF control law consists of linear and nonlinear feedback laws without any switching element [24,25]. The linear part is designed to yield small damping ratio to achieve a quick response. On the other hand, the nonlinear part is used to gradually change the damping ratio of the closed-loop system as the system output approaches the reference output so as to reduce the overshoot caused by the linear part [26,27]. In [28], an enhanced CNF technique with an integral term is introduced to remove the steady-state bias caused by unknown constant disturbances. In [26], a robust CNF control method is proposed to achieve fast and accurate set-point tracking for disturbed linear systems. The drawbacks of [26] and [28] are that the disturbance input is assumed constant and no parametric uncertainty is considered for the system. A CNF-based adaptive second-order sliding mode controller is proposed in [29] to enhance the transient performance of uncertain single-input-single-output (SISO) systems. In [30], the ISM and CNF methods are combined for robust tracking of a linear SISO system with time-varying disturbances. In [24], the algebraic Riccati equation (ARE) and CNF techniques are used for robust tracking and model following of a class of linear systems with time-varying uncertainties. However, these approaches require a Lyapunov equality which is a very conservative condition [31]. In [32], a new nonlinear sliding surface is proposed for a terminal sliding mode controller to achieve robustness and high-performance tracking of the disturbed systems; however, only the boundedness conditions on the state error are proven. To the best of the authors' knowledge, the problem of combination of ISM and CNF methods for fast and accurate robust tracking control of linear uncertain systems with time-varying disturbances and multiple time-delays is still open in the literature. Furthermore, very little efforts have been made in the performance improvement of robust tracking and obtaining less conservative linear matrix inequality (LMI) conditions for the CNF method. This motivates the current research.

In this paper, we consider the robust tracking and model following problem for linear MIMO systems with time-varying uncertain parameters, external disturbances and multiple delayed state perturbations. We employ an ISM controller combined with CNF control law such that the resulting controlled output would track a target reference as fast as possible without any steady-state bias. The CNF structure used in the proposed ISM-CNF allows for tracking the reference trajectory within a given accuracy, and the invariance property of ISM method allows for rejecting the disturbances. Using the Lyapunov–Krasovskii functional, we derive the asymptotic stability conditions in the form of a LMI. Unlike previous works, the resulting LMI conditions have much less pre-assumed design parameters, and consequently, the proposed method yields less conservative conditions. We offer the design procedure of the CNF law with a new form of the nonlinear function to improve the tracking performance of the closed-loop system. A minimization problem is numerically solved using the modified random search (MRS) algorithm, and then, the parameters of the nonlinear function are optimally tuned.

The organization of the paper is as follows: In Sect. 2, the problem of robust tracking and model following is stated, and the required assumptions are discussed. The main theoretical results are developed in Sect. 3. The selection of the nonlinear function in CNF for performance improvement of the overall system is discussed in Sect. 4. The simulation results are illustrated in Sect. 5, and conclusions are given in Sect. 6.

2 System description and assumptions

Consider a linear uncertain system with multiple time-delays and external disturbances as:

$$\begin{aligned} \dot{x}(t) &= [A + \Delta A(r(t))]x(t) \\ &\quad + \sum_{i=1}^{N_1} \Delta A_{di}(v(t))x(t - \tau_i(t)) \\ &\quad + [B + \Delta B(p(t))]u(t) + W(q(t)) \\ y(t) &= Cx(t), \end{aligned} \quad (1)$$

where $t \in [t_0, \infty)$, $x(t) \in R^n$ is the measurable state vector, $u(t) \in R^m$ is the control input, A , B , C are constant matrices of appropriate dimensions, $y(t) \in R^p$ is the output vector which is to track the reference output $y_m(t)$, and the matrices $\Delta A(\cdot)$, $\Delta B(\cdot)$,

and $\Delta A_{di}(\cdot), i = 1, \dots, N_1$ denote the time-varying uncertainties and are continuous in all their arguments. Moreover, $\tau_i(t) \in R^+$ is the time-varying delay and the vector $W(q(t)) \in R^n$ is the external disturbance. The uncertain functions $r(t), p(t), v(t)$ and $q(t)$ are Lebesgue measurable functions which belong to a compact bounding set Ω .

The objective is to design an ISM-CNF controller such that the controlled output $y(t)$ can track the reference output $y_m(t)$, in the presence of uncertainties and without experiencing large overshoot, and retain the invariance property of ISM method in rejecting disturbances.

The reference model is given by differential equations of the form [33]:

$$\begin{aligned} \dot{x}_m(t) &= A_m x_m(t) \\ y_m(t) &= C_m x_m(t), \end{aligned} \tag{2}$$

where A_m and C_m are constant matrices with appropriate dimensions, $x_m(t) \in R^{n_m}$ is the state vector of the reference model which is considered to be bounded, i.e., there exists a positive constant M_1 such that $\|x_m(t)\| \leq M_1$ for all $t \geq t_0$. We also assume that there exist matrices $G \in R^{n \times n_m}$ and $H \in R^{m \times n_m}$ satisfying [34, 35]:

$$\begin{bmatrix} A & B \\ C & 0 \end{bmatrix} \begin{bmatrix} G \\ H \end{bmatrix} = \begin{bmatrix} G A_m \\ C_m \end{bmatrix}. \tag{3}$$

If the solution of this algebraic equation cannot be found, a different reference model must be chosen. Moreover, the following assumptions on the original system are required:

Assumption 1 There exist continuous and bounded matrix functions $N(\cdot), E(\cdot), N_{di}(\cdot)$ and $\tilde{W}(\cdot)$ of appropriate dimensions such that [35]:

$$\begin{aligned} \Delta A(r(t)) &= B N(r(t)), \\ \Delta B(p(t)) &= B E(p(t)), \\ \Delta A_{di}(v(t)) &= B N_{di}(v(t)), \\ W(q(t)) &= B \tilde{W}(q(t)). \end{aligned} \tag{4}$$

This assumption is known as the matching condition on the uncertainties. For convenience, the following notations which represent the bounds of the uncertainties are introduced:

$$\begin{aligned} \rho_r &= \max_{r \in \Omega} \|N(r(t))\|, \\ \mu &= \max_{s \in \Omega} \|E(p(t))\|, \\ \rho_{vi} &= \max_{v \in \Omega} \|N_{di}(v(t))\|, \\ \rho_q &= \max_{q \in \Omega} \|\tilde{W}(q(t))\|. \end{aligned} \tag{5}$$

Assumption 2 For every $t \geq t_0$, μ satisfies $1 > \mu > 0$.

3 Main results

The output tracking error $e(t)$ and a new auxiliary state vector $\tilde{x}(t)$ are defined as [36]:

$$e(t) = y(t) - y_m(t), \tag{6}$$

$$\tilde{x}(t) = x(t) - G x_m(t), \tag{7}$$

where G is found from (3). From (1), (2), (3), (6) and (7), one can obtain:

$$\begin{aligned} e(t) &= C(x(t) - G x_m(t)) \\ &= C \tilde{x}(t). \end{aligned} \tag{8}$$

It follows from (8) that [37]:

$$\begin{aligned} \|e(t)\| &= \|C \tilde{x}(t)\| \\ &\leq \|C\| \|\tilde{x}(t)\|. \end{aligned} \tag{9}$$

Since $\|C\| \leq \infty$, one can conclude that $\|\tilde{x}(t)\| \rightarrow 0$ yields $\|e(t)\| \rightarrow 0$. Hence, the proof of the stability of $\|\tilde{x}(t)\|$ is sufficient for the tracking goal.

In this section, we propose the ISM-CNF control technique such that the resulting controlled output would track target reference as fast as possible without any steady-state bias. The design will be performed in four steps. In the first step, a linear feedback control law is designed. In the second step, the nonlinear feedback control is designed. In the third step, the linear and nonlinear feedback laws are combined to form the CNF control law, and in the final step, the discontinuous control law is added to the CNF controller for enforcing the sliding motion.

The linear feedback control law for system (1) has the form [33]:

$$u_L(t) = K x(t) + (H - K G) x_m(t), \tag{10}$$

where K is a gain matrix. Moreover, consider the nonlinear feedback control law as:

$$u_N(t) = \psi(\tilde{x}(t))B^T P \tilde{x}(t), \tag{11}$$

where P is a positive symmetrical matrix, and $\psi(\tilde{x}(t))$ is a non-positive locally Lipschitz function in $\tilde{x}(t)$ to be designed, which changes the damping ratio of the closed-loop system as the controlled output approaches the reference output in order to reduce the overshoot caused by the linear part.

The linear and nonlinear feedback control laws in (10) and (11) are combined to form a CNF control law as follows:

$$\begin{aligned} \kappa(\tilde{x}, t) &= u_L(t) + u_N(t) \\ &= K\tilde{x}(t) + Hx_m(t) + \psi(\tilde{x}(t))B^T P \tilde{x}(t). \end{aligned} \tag{12}$$

Driving System (1) by the CNF controller (12), yields the following dynamic equation for the closed-loop system:

$$\begin{aligned} \dot{\tilde{x}}(t) &= \left[A + BK + \Delta A(r(t)) + (B + \Delta B(p(t))) \right. \\ &\quad \left. \times \psi(\tilde{x}(t))B^T P + \Delta B(p(t))K \right] \tilde{x}(t) \\ &\quad + \sum_{i=1}^{N_1} \Delta A_{di}(v(t))\tilde{x}(t - \tau_i(t)) \\ &\quad + g(r, p, q, v, x_m), \end{aligned} \tag{13}$$

where:

$$\begin{aligned} g(r, p, q, v, x_m) &= [\Delta A(r(t))G + \Delta B(p(t))H] x_m(t) \\ &\quad + \sum_{i=1}^{N_1} \Delta A_{di}(v(t))Gx_m(t - \tau_i(t)) \\ &\quad + W(q(t)). \end{aligned} \tag{14}$$

Then, using Assumption 1, Eq. (14) can be written as:

$$g(r, p, q, v, x_m) = BF(r, p, q, v, x_m), \tag{15}$$

where:

$$\begin{aligned} F(r, p, q, v, x_m) &= [N(r(t))G + E(p(t))H] x_m(t) \\ &\quad + \sum_{i=1}^{N_1} N_{di}(v(t))Gx_m(t - \tau_i(t)) \\ &\quad + \tilde{W}(q(t)). \end{aligned} \tag{16}$$

Furthermore, defining the bound:

$$\begin{aligned} \rho &= \max \{ \|F(r, p, q, v, x_m)\| : \\ &\quad r, p, q, v, x_m \in \Omega, \|x_m(t)\| \leq M \}, \end{aligned} \tag{17}$$

and using (5), one can write that:

$$\rho \leq [\rho_r \|G\| + \mu \|H\|]M_1 + \sum_{i=1}^{N_1} \rho_{vi} \|G\| M_1 + \rho_q. \tag{18}$$

In this paper, the function $\psi(\tilde{x}(t))$ in (11) is defined as:

$$\psi(\tilde{x}(t)) = -\frac{\varphi^2}{(1 + \mu) [\|B^T P \tilde{x}(t)\| \varphi + \sigma(\tilde{x}(t))]}, \tag{19}$$

where $\varphi = \rho + \rho_r \|\tilde{x}(t)\| + \sum_{i=1}^{N_1} \rho_{vi} \|\tilde{x}(t - \tau_i(t))\|$ and $\sigma(\tilde{x}(t)) \in R^+$ is any positive uniformly continuous and bounded function that satisfies:

$$\lim_{t \rightarrow \infty} \int_{t_0}^t \sigma(\tilde{x}(\tau))d\tau \leq \bar{\sigma} < \infty, \tag{20}$$

where $\bar{\sigma}$ is any positive constant. The selection procedure of $\sigma(\tilde{x}(t))$ will be discussed later.

Remark 1 Considering (11) and (19) and since $\sigma(\tilde{x}(t)) > 0$, one can derive:

$$\begin{aligned} \|u_N(t)\| &= \frac{\left(\rho + \rho_r \|\tilde{x}(t)\| + \sum_{i=1}^{N_1} \rho_{vi} \|\tilde{x}(t - \tau_i(t))\| \right)^2 \|B^T P \tilde{x}(t)\|}{(1 + \mu) \left[\|B^T P \tilde{x}(t)\| \left(\rho + \rho_r \|\tilde{x}(t)\| + \sum_{i=1}^{N_1} \rho_{vi} \|\tilde{x}(t - \tau_i(t))\| \right) + \sigma(\tilde{x}(t)) \right]} \\ &\leq \frac{\left(\rho + \rho_r \|\tilde{x}(t)\| + \sum_{i=1}^{N_1} \rho_{vi} \|\tilde{x}(t - \tau_i(t))\| \right)}{1 + \mu}, \end{aligned} \tag{21}$$

which shows that the nonlinear control law (11) is uniformly bounded.

The following nonlinear integral-type sliding surface is proposed to make the overall system robust:

$$s(\tilde{x}, t) = L \left\{ \tilde{x}(t) - \tilde{x}(0) - \int_0^t (A\tilde{x}(\tau) + B\kappa(\tilde{x}, \tau))d\tau \right\}, \tag{22}$$

where $L \in R^{m \times n}$ is a constant matrix, and the additional integral term provides one more degree of freedom in design than the linear sliding surface. Furthermore, the sliding surface (22) provides a general framework to eliminate the reaching phase such that the sliding mode exists from the initial time $t = 0$, and thus, the system response becomes completely invariant against uncertainties.

3.1 Integral sliding mode controller design

The following theorem guarantees the existence of sliding mode control for robust tracking and model following of the uncertain dynamical system (1).

Theorem 1 Consider the uncertain system (1). Applying the control law as:

$$u(t) = \begin{cases} \kappa(\tilde{x}, t) - (\eta + M(x, t)) \frac{(LB)^T s}{\|(LB)^T s\|}, & \text{if } s \neq 0 \\ \kappa(\tilde{x}, t), & \text{if } s = 0 \end{cases} \tag{23}$$

where $\eta > 0$ and $M(x, t)$ given by:

$$M(x, t) = \frac{1}{1 - \mu} \left\{ \left[\rho_r + \mu \|K\| + \sum_{i=1}^{N_1} \rho_{vi} q_i \right] \|\tilde{x}(t)\| - \mu \psi(\tilde{x}(t)) \left\| B^T P \tilde{x}(t) \right\| + \|Hx_m(t)\| + \rho + \vartheta \right\}, \tag{24}$$

where ϑ is chosen to be some positive constant, then the trajectory of system (1) is guaranteed to be kept on the sliding surface from any initial condition.

Proof Consider the following Lyapunov function candidate:

$$V_1(\tilde{x}, t) = \frac{1}{2} s^T(\tilde{x}, t) s(\tilde{x}, t). \tag{25}$$

Taking the derivative of the sliding surface (22) along the trajectories of system (1) yields:

$$\begin{aligned} \dot{s}(\tilde{x}, t) &= L \left\{ \dot{\tilde{x}}(t) - A\tilde{x}(t) - B\kappa(\tilde{x}, t) \right\} \\ &= L \left\{ \left[BK + \Delta A(r(t)) + \Delta B(p(t))K \right. \right. \\ &\quad \left. \left. + (B + \Delta B(p(t))) \psi(\tilde{x}(t)) B^T P \right] \tilde{x}(t) \right. \\ &\quad \left. + g(r, p, q, x_m) + \sum_{i=1}^{N_1} \Delta A_{di}(v(t)) \tilde{x}(t - \tau_i(t)) \right. \\ &\quad \left. - (B + \Delta B(p(t))) (\eta + M(x, t)) \right. \\ &\quad \left. \times \frac{(LB)^T s}{\|(LB)^T s\|} - B\kappa(\tilde{x}, t) \right\} \\ &= LB \{ [N(r(t)) + E(p(t))K \\ &\quad + E(p(t))\psi(\tilde{x}(t))B^T P] \tilde{x}(t) \\ &\quad + F(r, p, q, x_m) + \sum_{i=1}^{N_1} N_{di}(v(t)) \tilde{x}(t - \tau_i(t)) \\ &\quad - (I + E(p(t))) (\eta + M(x, t)) \\ &\quad \times \frac{(LB)^T s}{\|(LB)^T s\|} - Hx_m(t) \}. \end{aligned} \tag{26}$$

Differentiating the Lyapunov function (25) with respect to time and substituting (23), (24) and (26) in the result yields:

$$\begin{aligned} \dot{V}_1 &= s^T \dot{s} \leq \left\{ (\rho_r + \mu \|K\|) \|\tilde{x}(t)\| \right. \\ &\quad \left. - \mu \psi(\tilde{x}(t)) \left\| B^T P \tilde{x}(t) \right\| + \|F(r, p, q, x_m)\| \right. \\ &\quad \left. + \sum_{i=1}^{N_1} \|N_{di}(v(t))\| \|\tilde{x}(t - \tau_i(t))\| + \|Hx_m(t)\| \right. \\ &\quad \left. - (1 - \mu) (\eta + M(x, t)) \right\} \|(LB)^T s\|. \end{aligned} \tag{27}$$

From the Razumikhin Theorem [1], one can write:

$$\|\tilde{x}(t - \tau_i(t))\| \leq q_i \|\tilde{x}(t)\|, \quad q_i > 1 \quad (i = 1, \dots, N_1). \tag{28}$$

Then, we conclude that:

$$\begin{aligned} \dot{V}_1 &\leq \left[\left(\rho_r + \mu \|K\| + \sum_{i=1}^{N_1} \rho_{vi} q_i \right) \|\tilde{x}(t)\| \right. \\ &\quad - \mu \psi(\tilde{x}(t)) \left\| B^T P \tilde{x}(t) \right\| + \rho + \|Hx_m(t)\| \\ &\quad \left. - (1 - \mu)(\eta + M(x, t)) \right\| (LB)^T s \Big\| \\ &\leq -\vartheta \left\| (LB)^T s \right\| < 0 \end{aligned} \tag{29}$$

Therefore, the controller (23) using function (24) guarantees that the sliding mode can be maintained for all $t \geq t_0$.

In the following, the condition for the asymptotic tracking of (13) is provided in the form of an LMI, and consequently, the stability of the nonlinear integral-type sliding surface is proven.

Theorem 2 Consider the closed-loop system (13) with the time-varying delays $\tau_i(t)$ bounded by scalars ζ_i where $|\dot{\tau}_i(t)| \leq \zeta_i < 1$. Suppose that Assumptions 1 and 2 are satisfied. If there exist matrices $S_i > 0, i = 1, \dots, N_1, X > 0$, and Y with appropriate dimensions such that:

$$\begin{pmatrix} AX + XA^T + (1 + \mu)[BY + Y^T B^T] + \sum_{i=1}^{N_1} S_i & 0 & \dots & 0 \\ * & -(1 - \zeta_1)S_1 & 0 & 0 \\ * & * & \ddots & 0 \\ * & * & * & -(1 - \zeta_{N_1})S_{N_1} \end{pmatrix} < 0, \tag{30}$$

then using $K = YX^{-1}$ and $P = X^{-1}$ in (10) and (11), respectively, the CNF control law (12) guarantees that the output $y(t)$ asymptotically tracks the reference output $y_m(t)$.

Proof Constructing the Lyapunov–Krasovskii functional candidate as:

$$V_2(\tilde{x}, t) = \tilde{x}^T(t)P\tilde{x}(t) + \sum_{i=1}^{N_1} \int_{t-\tau_i}^t \tilde{x}^T(\beta)R_i\tilde{x}(\beta)d\beta, \tag{31}$$

where the real symmetrical matrix $R_i > 0$ is determined using the LMI. Taking the derivative of (31) along the trajectories of the closed-loop system in (13) yields:

$$\begin{aligned} \dot{V}_2(\tilde{x}, t) &= \dot{\tilde{x}}^T(t)P\tilde{x}(t) + \tilde{x}^T(t)P\dot{\tilde{x}}(t) + \sum_{i=1}^N \tilde{x}^T(t)R_i\tilde{x}(t) \\ &\quad - \sum_{i=1}^N (1 - \zeta_i)\tilde{x}^T(t - \tau_i(t))R_i\tilde{x}(t - \tau_i(t)) \\ &= \tilde{x}^T(t) \left[P(A + BK) + (A + BK)^T P \right. \\ &\quad \left. + PBN + (PBN)^T + PBEK + (PBEK)^T \right. \\ &\quad \left. + PB(2I + E + E^T)\psi(\tilde{x}(t))B^T P \right] \tilde{x}(t) \\ &\quad + \tilde{x}^T PBF + F^T B^T P \tilde{x} \\ &\quad + \left[B \sum_{i=1}^{N_1} N_{di}(v(t))\tilde{x}(t - \tau_i(t)) \right]^T P \tilde{x}(t) \\ &\quad + \tilde{x}^T(t)PB \sum_{i=1}^{N_1} N_{di}(v(t))\tilde{x}(t - \tau_i(t)) \\ &\quad + \sum_{i=1}^N \tilde{x}^T(t)R_i\tilde{x}(t) - \sum_{i=1}^N (1 - \zeta_i)\tilde{x}^T \\ &\quad \times (t - \tau_i(t))R_i\tilde{x}(t - \tau_i(t)). \end{aligned} \tag{32}$$

In the light of Assumption 1, one can obtain that:

$$\begin{aligned} \dot{V}_2(\tilde{x}, t) &\leq \tilde{x}^T(t) \left[PA + A^T P + (1 + \mu) \right. \\ &\quad \left. \times (PBK + K^T B^T P) \right] \tilde{x}(t) + \sum_{i=1}^N \tilde{x}^T(t)R_i\tilde{x}(t) \\ &\quad - \sum_{i=1}^N (1 - \zeta_i)\tilde{x}^T(t - \tau_i(t))R_i\tilde{x}(t - \tau_i(t)) \\ &\quad + 2 \left\| B^T P \tilde{x}(t) \right\| \sum_{i=1}^{N_1} \rho_{vi} \|\tilde{x}(t - \tau_i(t))\| \\ &\quad + 2(\rho_r \|\tilde{x}(t)\| + \rho) \left\| B^T P \tilde{x}(t) \right\| \\ &\quad + 2(1 + \mu)\tilde{x}^T(t)PB\psi(\tilde{x}(t))B^T P \tilde{x}(t). \end{aligned} \tag{33}$$

Substituting (19) in (33) yields:

$$\begin{aligned}
 \dot{V}_2(\tilde{x}, t) &\leq \Psi^T Q \Psi + 2 \left(\rho + \rho_r \|\tilde{x}(t)\| + \sum_{i=1}^{N_1} \rho_{vi} \|\tilde{x}(t - \tau_i(t))\| \right) \left\| B^T P \tilde{x}(t) \right\| \\
 &\quad - 2 \frac{\left(\rho + \rho_r \|\tilde{x}(t)\| + \sum_{i=1}^{N_1} \rho_{vi} \|\tilde{x}(t - \tau_i(t))\| \right)^2}{\left\| B^T P \tilde{x}(t) \right\| \left(\rho + \rho_r \|\tilde{x}(t)\| + \sum_{i=1}^{N_1} \rho_{vi} \|\tilde{x}(t - \tau_i(t))\| \right) + \sigma(\tilde{x}(t))} \left\| B^T P \tilde{x}(t) \right\|^2 \\
 &= \Psi^T Q \Psi + 2 \frac{\left(\rho + \rho_r \|\tilde{x}(t)\| + \sum_{i=1}^{N_1} \rho_{vi} \|\tilde{x}(t - \tau_i(t))\| \right) \left\| B^T P \tilde{x}(t) \right\| \sigma(\tilde{x}(t))}{\left\| B^T P \tilde{x}(t) \right\| \left(\rho + \rho_r \|\tilde{x}(t)\| + \sum_{i=1}^{N_1} \rho_{vi} \|\tilde{x}(t - \tau_i(t))\| \right) + \sigma(\tilde{x}(t))}.
 \end{aligned} \tag{34}$$

where $\Psi = [\tilde{x}(t) \ \tilde{x}(t - \tau_1(t)) \ \dots \ \tilde{x}(t - \tau_{N_1}(t))]$ and

$$Q = \begin{pmatrix} PA + A^T P + (1 + \mu)[PBK + K^T B^T P] + \sum_{i=1}^{N_1} R_i & 0 & \dots & 0 \\ * & -(1 - \zeta_1)R_1 & 0 & 0 \\ * & * & \ddots & 0 \\ * & * & * & -(1 - \zeta_{N_1})R_{N_1} \end{pmatrix}.$$

Assuming $X = P^{-1}$, $S_i = X R_i X$ and pre- and post-multiplying Q by X , LMI (30) is obtained.

Considering the fact that:

$$0 \leq \frac{\sigma\theta}{\sigma + \theta} \leq \sigma, \quad \forall \sigma, \theta > 0, \tag{35}$$

the last term in (34) becomes less than 2σ , and thus it follows that:

$$\dot{V}_2(\tilde{x}, t) \leq \lambda_{\min}(Q) \|\Psi\|^2 + 2\sigma(\tilde{x}(t)). \tag{36}$$

On the other hand, there always exist two positive constants c_1 and c_2 such that:

$$c_1 \|\tilde{x}(t)\|^2 \leq V_2(\tilde{x}(t)) \leq c_2 \|\tilde{x}(t)\|^2. \tag{37}$$

From (36) and (37), one can obtain:

$$\begin{aligned}
 0 &\leq c_1 \|\tilde{x}(t)\|^2 \leq V_2(\tilde{x}(t)) \\
 &= V_2(\tilde{x}(t_0)) + \int_{t_0}^t \dot{V}_2(\tilde{x}(\tau)) d\tau
 \end{aligned}$$

$$\begin{aligned}
 &\leq c_2 \|\tilde{x}(t_0)\|^2 + \int_{t_0}^t \lambda_{\min}(Q) \|\Psi(\tau)\|^2 d\tau \\
 &\quad + 2 \int_{t_0}^t \sigma(\tilde{x}(\tau)) d\tau,
 \end{aligned} \tag{38}$$

and hence:

$$0 \leq c_1 \|\tilde{x}(t)\|^2 \leq c_2 \|\tilde{x}(t_0)\|^2 + 2 \int_{t_0}^t \sigma(\tilde{x}(\tau)) d\tau. \tag{39}$$

Notice that for $t \geq t_0$, we have:

$$\sup_{t \in [t_0, \infty)} \int_{t_0}^t \sigma(\tilde{x}(\tau)) d\tau \leq \bar{\sigma}, \tag{40}$$

where using (40) in (39) yields:

$$0 \leq c_1 \|\tilde{x}(t)\|^2 \leq c_2 \|\tilde{x}(t_0)\|^2 + 2\bar{\sigma}. \tag{41}$$

Moreover, taking the limit of (38) as t approaches infinity, follows that:

$$0 \leq c_2 \|\tilde{x}(t_0)\|^2 + \lim_{t \rightarrow \infty} \int_{t_0}^t \lambda_{\min}(Q) \|\Psi(\tau)\|^2 d\tau + 2 \lim_{t \rightarrow \infty} \int_{t_0}^t \sigma(\tilde{x}(\tau)) d\tau. \tag{42}$$

Form (20) and (42), one can obtain:

$$- \lim_{t \rightarrow \infty} \int_{t_0}^t \lambda_{\min}(Q) \|\Psi(\tau)\|^2 d\tau \leq c_2 \|\tilde{x}(t_0)\|^2 + 2\bar{\sigma}. \tag{43}$$

It follows from (41) that $\tilde{x}(t)$ is uniformly bounded. Since $\tilde{x}(t)$ is continuous, it is uniformly continuous, and therefore, the term $\lambda_{\min}(Q) \|\Psi(t)\|^2$ in (43) is also uniformly continuous. Applying the Barbalat Lemma to (43) results in:

$$\lim_{t \rightarrow \infty} \lambda_{\min}(Q) \|\Psi(t)\|^2 = 0. \tag{44}$$

Because $\lambda_{\min}(Q) < 0$, one can conclude that:

$$\lim_{t \rightarrow \infty} \|\Psi(t)\| = 0. \tag{45}$$

Therefore, the closed-loop system described by (13) is uniformly bounded and its auxiliary state $\tilde{x}(t)$ uniformly asymptotically converges to zero. Then, it can be obtained from (9) that the tracking error $e(t)$ decreases asymptotically toward zero. \square

3.2 Robust performance analysis

For any control problem to have satisfactory behavior, two objectives must be achieved, namely stability and performance [38]. The control law (23) is designed so as to satisfy asymptotic stability in the Lyapunov sense and the performance measure in L_2 sense satisfying:

$$\int_0^T \|s\|^2 dt \leq \zeta^2 \int_0^T \|\tilde{W}\|^2 dt, \tag{46}$$

for some $\zeta > 0$, $T \geq 0$, and all $\tilde{W} \in L_2(0, T)$. To prove (46), the following inequality holds:

$$- (\zeta \tilde{W} - s)^T (\zeta \tilde{W} - s) \leq 0. \tag{47}$$

Form (47), one can obtain:

$$\|s\| - \zeta^2 \|\tilde{W}\|^2 \leq 2\|s\|^2 - 2\zeta s^T \tilde{W}. \tag{48}$$

Then, it follows from (29) and (48) that:

$$\begin{aligned} \int_0^T (\|s\| - \zeta^2 \|\tilde{W}\|^2) dt &\leq \int_0^T 2(\|s\|^2 - \zeta s^T \tilde{W}) dt \\ &\leq \int_0^T [2(\|s\|^2 - \zeta s^T \tilde{W}) + \dot{V}_1] dt - (V_1(T) - V_1(0)) \\ &\leq \int_0^T [2(\|s\|^2 - \zeta s^T \tilde{W}) - \vartheta \|(LB)^T s\|] dt \\ &\leq \int_0^T \|s\| (2\|s\| + 2\zeta \|\tilde{W}\| - \vartheta \|LB\|) dt. \end{aligned} \tag{49}$$

Using (22), the sufficient condition to guarantee inequality (49) is derived as follows:

$$\begin{aligned} \|s\| &= \left\| L\tilde{x}(t) - L\{\tilde{x}(0) + \int_0^t (A\tilde{x}(\tau) + B\kappa(\tilde{x}, \tau)) d\tau\} \right\| \\ &\leq \|L\| \|\tilde{x}(t) - \tilde{x}(0)\| + \|L\| \\ &\times \left\| \int_0^t [(A + BK + \psi(\tilde{x})B^T P)\tilde{x}(\tau) + BHx_m(\tau)] d\tau \right\| \\ &\leq \|L\| \left(\|\tilde{x}(t)\| + \|\tilde{x}(0)\| + \|A + BK\| \left\| \int_0^t \tilde{x}(\tau) d\tau \right\| \right. \\ &\quad \left. + \|BH\| \left\| \int_0^t x_m(\tau) d\tau \right\| + \left\| \int_0^t \psi(\tilde{x})B^T P\tilde{x}(\tau) d\tau \right\| \right). \end{aligned} \tag{50}$$

Now assuming $\max \|\tilde{x}(t)\| \leq \aleph$, it follows from (21) and (50) that $\|s\| \leq \Im$, where:

$$\begin{aligned} \Im &= \|L\| (\aleph + \|\tilde{x}(0)\| + \|A + BK\| \aleph T + \|BH\| M_1 T \\ &\quad + \frac{T}{1 + \mu} \left(\rho + \rho_r \aleph + \sum_{i=1}^{N_1} \rho_{vi} q_i \aleph \right)). \end{aligned} \tag{51}$$

Therefore, the inequalities (46) and (49) can be accomplished by appropriately choosing the sliding variable ϑ that satisfies:

$$\vartheta \geq \frac{2\Im + 2\zeta \rho q}{\|LB\|}. \tag{52}$$

4 Selection of the nonlinear function $\sigma(\tilde{x}(t))$

The required properties of the nonlinear function $\sigma(\tilde{x}(t))$ and some of its examples are discussed in [24].

To adapt the variation of the tracking target, the nonlinear function is chosen as:

$$\sigma(\tilde{x}(t)) = \beta e^{\frac{-\alpha_0 \alpha}{\|y(t) - y_m(t)\|}}, \tag{53}$$

where

$$\alpha_0 = \begin{cases} \|y(t_0) - y_m(t)\|, & y(t_0) \neq y_m(t) \\ 1, & y(t_0) = y_m(t) \end{cases} \tag{54}$$

and α and β are the positive scalars which can be tuned to yield a desired performance, i.e., fast settling time and small steady-state error. The nonlinear function $\sigma(\tilde{x}(t))$ smoothly varies from the initial value $\beta e^{-\alpha}$ to the steady-state value 0 as $\|y(t) - y_m(t)\|$ tends to zero. As it is clear from (54), the scaling parameter α_0 changes for different values of the tracking target $y_m(t)$, and consequently, the initial value of the nonlinear function $\sigma(\tilde{x}(t))$ does not depend on the tracking target $y_m(t)$.

Since we consider a tracking-control problem, a direct and simple performance index is the integral of absolute-value of error (IAE) with the following formula:

$$\text{IAE} = \int_0^{t_f} |e| dt, \tag{55}$$

where t_f represents the total running time. Also, to address the settling time and overshoot of the transient response, the integral of time-multiplied absolute-value of error (ITAE) is presented:

$$\text{ITAE} = \int_0^{t_f} t |e| dt. \tag{56}$$

To show the consumption of energy, the integral of the square value (ISV) of the control input is represented by the following formula [39]:

$$\text{ISV} = \int_0^{t_f} u^2(t) dt. \tag{57}$$

In the following, the optimized parameters α and β of the nonlinear function (53) are determined. To evaluate the performance of the closed-loop system, a multi-objective performance criterion is chosen which includes steady-state error E_{ss} and IAE and ISV indices. The proposed cost function is considered as follows [40]:

$$f(\chi) = w_1 \text{IAE} + w_2 \text{ISV} + w_3 E_{ss}, \tag{58}$$

where $w_i, i = 1, \dots, 3$ are the desired weighting parameters and $\chi = [\alpha, \beta]^T$ is the solution point.

Since the closed-loop system is nonlinear, the minimization problem (58) is numerically solved using MRS algorithm, which is a direct-search-based method. The MRS method involves the following steps:

- Step 1:** Choose a starting point χ as the current point, and b as a bias which is initially set equal to zero.
- Step 2:** Evaluate the objective function at the new point $\chi + b + d\chi$ where $d\chi$ is a random vector.
- Step 3:** If $f(\chi + b + d\chi) < f(\chi)$, set the current point χ equal to $\chi + b + d\chi$ and the bias term b equal to $0.2b + 0.4d\chi$ then jump to step 6.
- Step 4:** If $f(\chi + b - d\chi) < f(\chi)$, set the current point χ equal to $\chi + b - d\chi$ and the bias term b equal to $b - 0.4d\chi$ then jump to step 6.
- Step 5:** Set the bias term equal to $0.5b$.
- Step 6:** If the maximum number of function evaluations is not reached return to step 2.

Remark 2 The chattering phenomenon is due to the presence of the sign function in the switching term, and it can cause the control input to start oscillating around the zero sliding surface, resulting in unwanted wear and tear of the actuators [41]. In order to reduce chattering in the actual implementation, the discontinuous function $\frac{(LB)^T s}{\|(LB)^T s\|}$ in (23) is replaced by a smoothing continuous function of the form $\frac{(LB)^T s}{\|(LB)^T s\| + \hbar}$, where \hbar is a small positive constant.

Remark 3 To attenuate the chattering behavior, the unit vector function $\frac{(LB)^T s}{\|(LB)^T s\|}$ in the control law (23) should be replaced by the saturation function $\text{sat}\left(\frac{(LB)^T s}{\varepsilon}\right)$, where $\varepsilon > 0$ is a small scalar. It can be visualized that as $\varepsilon \rightarrow 0$, the function $\text{sat}\left(\frac{(LB)^T s}{\varepsilon}\right)$ tends to the unit vector function. The variable ε can be used to trade off the requirement of maintaining ideal performance with that of ensuring a smooth control action. Therefore, similar to [1, 30, 42–46], the control law (23) is modified as:

$$u(t) = \begin{cases} \kappa(\tilde{x}, t) - (\eta + M(x, t)) \\ \quad \times \text{sat}\left(\frac{(LB)^T s}{\varepsilon}\right), & \text{if } s \neq 0 \\ \kappa(\tilde{x}, t), & \text{if } s = 0 \end{cases} \tag{59}$$

where $\text{sat}(\cdot)$ is a saturation function and ε is the boundary layer thickness.

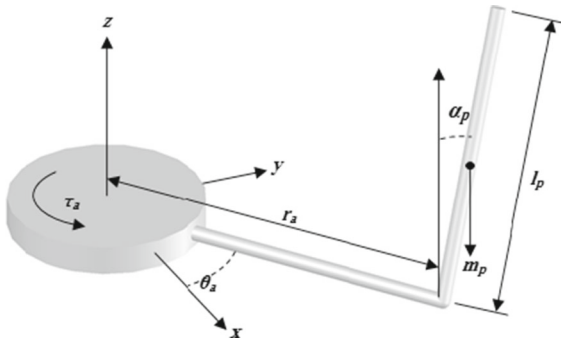


Fig. 1 Planar presentation of RIP system

Remark 4 For a more smooth change of the switching signal, a hyperbolic tangent function has also been used to introduce a thin boundary layer around the sliding surface as $\tanh\left(\frac{(LB)^T s}{\varepsilon}\right)$, where ε denotes thickness of the boundary layer. Hence, the control law (23) can be modified as:

$$u(t) = \kappa(\tilde{x}, t) - (\eta + M(x, t)) \tanh\left(\frac{(LB)^T s}{\varepsilon}\right). \tag{60}$$

5 Simulation results

To illustrate the usefulness of the proposed method, in this section, the following examples are considered. In *Example A*, we apply the proposed tracking method to a rotary inverted pendulum (RIP) system with uncertainty and time-varying delays due to non-symmetrical backlash and various frictions. In *Example B*, the vibration control of an uncertain time-delay system which is proposed in [1] is presented. In *Example C*, for the sake of comparison, we apply the proposed method to an uncertain system with multiple time-varying delays provided in [1, 34], and we compare the performance of the three controllers.

5.1 Example A: RIP system

The RIP system is a well-known test platform for evaluating control methods. Figure 1 shows the schematic diagram of an RIP system [40, 47].

Let α_p be the pendulum angle and θ_a be the arm angle. Also, let τ_a , u , l_p , m_p , r_a and J_b be the motor torque, control input, pendulum length, pendulum

mass, arm length and moment of inertia of the effective mass, respectively. The dynamic equations of this system considering time-varying delays, backlash and friction effects are [40]:

$$\begin{aligned} & (A_p + B_p \sin^2 \alpha_p) \ddot{\theta}_a + (C_p \cos \alpha_p) \ddot{\alpha}_p \\ & - (C_p \sin \alpha_p) \dot{\alpha}_p^2 + (B_p \sin 2\alpha_p) \dot{\alpha}_p \dot{\theta}_a \\ & + F_p \dot{\theta}_a + G_p \operatorname{sgn}(\dot{\theta}_a) + H_p \theta_a = I_p u \\ & + \frac{A_p B_p - C_p^2}{B_p} \sum_{i=1}^2 A_{di}(v(t)) \begin{bmatrix} \alpha_p(t - \tau_i) \\ \dot{\alpha}_p(t - \tau_i) \\ \theta_a(t - \tau_i) \\ \dot{\theta}_a(t - \tau_i) \end{bmatrix}, \end{aligned} \tag{61}$$

$$\begin{aligned} & B_p \ddot{\alpha}_p + (C_p \cos \alpha_p) \ddot{\theta}_a - (B_p \sin \alpha_p \cos \alpha_p) \dot{\theta}_a^2 \\ & - D_p \sin \alpha_p + E_p \dot{\alpha}_p = 0, \end{aligned} \tag{62}$$

where E_p , F_p , I_p , G_p and H_p are the pendulum damping constant, arm damping constant, control input coefficient, arm Coulomb friction and elasticity coefficients, respectively. The coefficients A_p , B_p , C_p and D_p are calculated as [48]:

$$\begin{aligned} A_p &= m_p r_a^2 + J_b, \quad B_p = \frac{1}{3} m_p l_p^2, \\ C_p &= \frac{1}{2} m_p r_a l_p, \quad D_p = \frac{1}{2} m_p g l_p. \end{aligned} \tag{63}$$

The parameters of nonlinear model of the whole system are given as follows [48]:

$$\begin{aligned} A_p &= 3.291, \quad B_p = 0.237, \quad C_p = 0.237, \quad D_p = 6.052, \\ E_p &= 0.0132, \quad F_p = 14.283, \quad G_p = 1.428, \quad H_p = 1.72, \\ I_p &= 141.32. \end{aligned}$$

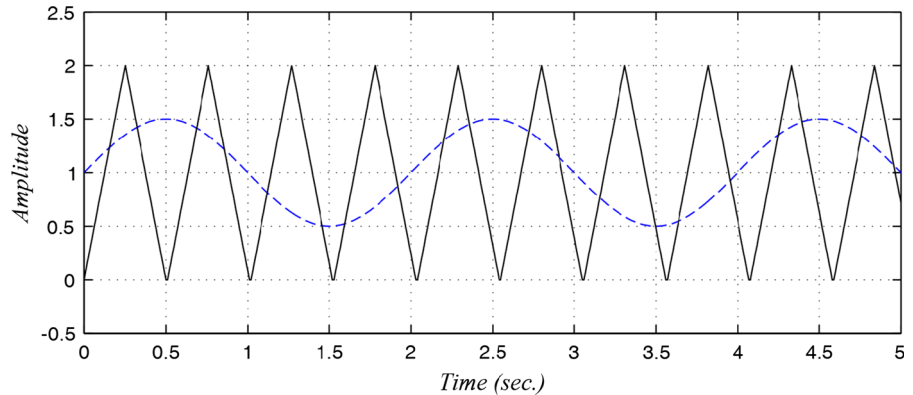
The nonlinear model of the RIP system demonstrated in (62)–(63) can be linearized around the unstable equilibrium point ($\alpha_p = \dot{\alpha}_p = \theta_a = \dot{\theta}_a = 0$) resulting in the following equation [47]:

$$\dot{x}(t) = Ax(t) + Bu(t), \tag{64}$$

where $x = [\alpha_p \ \dot{\alpha}_p \ \theta_a \ \dot{\theta}_a]^T$, and

$$\begin{aligned} A &= \frac{1}{A_p B_p - C_p^2} \begin{bmatrix} 0 & 1 & 0 & 0 \\ A_p D_p & -A_p E_p & C_p H_p & C_p F_p \\ 0 & 0 & 0 & 1 \\ -C_p D_p & C_p E_p & -B_p H_p & -B_p F_p \end{bmatrix}, \\ B &= \frac{1}{A_p B_p - C_p^2} [0 \ -C_p I_p \ 0 \ B_p I_p]^T. \end{aligned}$$

Fig. 2 The time-varying delays $\tau_1(t)$ (dashed) and $\tau_2(t)$ (solid)



Because of linearization of RIP system equations, higher-order terms are eliminated, and uncertainties, disturbances and time-varying delays in linearized model parameters must be considered in control approach. Thus, we encounter the following system:

$$\begin{aligned} \dot{x}(t) &= \left(\begin{bmatrix} 0 & 2.8 & 0 & 0 \\ 55.8 & -0.12 & 1.15 & 9.5 \\ 0 & 0 & 0 & 0 \\ -4.02 & 0.01 & -0.6 & -5.03 \end{bmatrix} + \Delta A(r(t)) \right) x(t) \\ &+ \sum_{i=1}^2 \Delta A_{di}(v(t))x(t - \tau_i(t)) \\ &+ \left(\begin{bmatrix} 0 \\ -94.32 \\ 0 \\ -4.02 \end{bmatrix} + \Delta B(p(t)) \right) u(t) + W(q(t)), \\ y(t) &= \begin{bmatrix} 0.5 & 0 & 0 & 0 \\ 0 & 0.5 & 0 & 0 \end{bmatrix} x(t), \end{aligned} \tag{65}$$

with disturbances r, p, q, v satisfying: $|r(t)| \leq 0.5$, $|p(t)| \leq 0.5$, $|q(t)| \leq 0.5$, $|v(t)| \leq 1.5$. Moreover, the reference model is given as:

$$\begin{aligned} \dot{x}_m(t) &= \begin{bmatrix} -5 & 0 & 0 & 0 \\ 0 & -5 & 0 & 0 \\ 0 & 0 & -5 & 0 \\ 0 & 0 & 0 & -5 \end{bmatrix} x_m(t), \\ y_m(t) &= \begin{bmatrix} 4.6 & 2.3 & 2.3 & 0 \\ -8.25 & -4.15 & -4.15 & 0 \end{bmatrix} x_m(t). \end{aligned} \tag{66}$$

Here, the matrices G and H can be obtained from (3) as follows:

$$\begin{aligned} G &= \begin{bmatrix} 9.3 & 4.6 & 4.6 & 0 \\ -16.5 & -8.3 & -8.3 & 0 \\ 21.8 & 10.9 & 10.9 & 0 \\ -38.8 & -19.4 & -19.4 & 0 \end{bmatrix}, \\ H &= [1 \ 0.5 \ 0.5 \ 0]. \end{aligned}$$

From (4) and (65), one can obtain: $N(r(t)) = r(t) [0.4 \ 0.7 \ 1 \ 1.5]$, $E(p(t)) = p(t)$, $\tilde{W}(q(t)) = q(t)$, $N_{d1}(v(t)) = v(t) [0.3 \ 0.7 \ 0.5 \ 0.4]$, $N_{d2}(v(t)) = v(t) [0.2 \ 0.4 \ 0.5 \ 0.8]$. Then, from (5) and (65), the following parameters are calculated: $\rho_r = 1$, $\mu = 0.5$, $\rho_q = 0.5$, $\rho_{v1} = 1.5$, $\rho_{v2} = 1.5$. The constant parameters are selected as: $w_1 = [0.4 \ 0.2]$, $w_2 = 0.02$, $w_3 = [1 \ 1]$, $\eta = 0.3$, $\varepsilon = 0.2$, $\vartheta = 0.5$, $L = [0.5 \ 1 \ 0 \ 1]$. For the simulation purposes, the uncertain time-varying parameters and their initial conditions are set as:

$$\begin{aligned} v(t) &= 1 + 0.5 \sin(2t), \quad p(t) = 0.5 \cos(2t), \\ q(t) &= 0.5 \sin(3t), \quad r(t) = 0.5 \sin(3t), \end{aligned}$$

$x(0) = [\pi \ -1 \ -3 \ 1]^T$, $x_m(0) = [2 \ -3 \ -0.5 \ 4]^T$, and the time-varying delays $\tau_1(t)$ and $\tau_2(t)$ are chosen as shown in Fig. 2, where $\tau_1(t) = 1 + 0.5 \sin(\pi t)$.

A solution of matrices P, K and $R_i, i = 1, 2$ in (30) is found using Matlab LMI toolbox as:

$$\begin{aligned} P &= \begin{bmatrix} 0.302 & 0.083 & 0.031 & 0.064 \\ 0.084 & 0.035 & 0.01 & 0.027 \\ 0.031 & 0.01 & 0.008 & 0.01 \\ 0.064 & 0.027 & 0.01 & 0.025 \end{bmatrix}, \\ R_1 = R_2 &= \begin{bmatrix} 3.7 & 1.09 & 0.379 & 0.826 \\ 1.09 & 0.35 & 0.117 & 0.27 \\ 0.379 & 0.117 & 0.043 & 0.09 \\ 0.826 & 0.27 & 0.09 & 0.212 \end{bmatrix}, \\ K &= [1.28 \ 0.22 \ 0.076 \ 0.22]. \end{aligned}$$

Fig. 3 The cost function $f(x)$

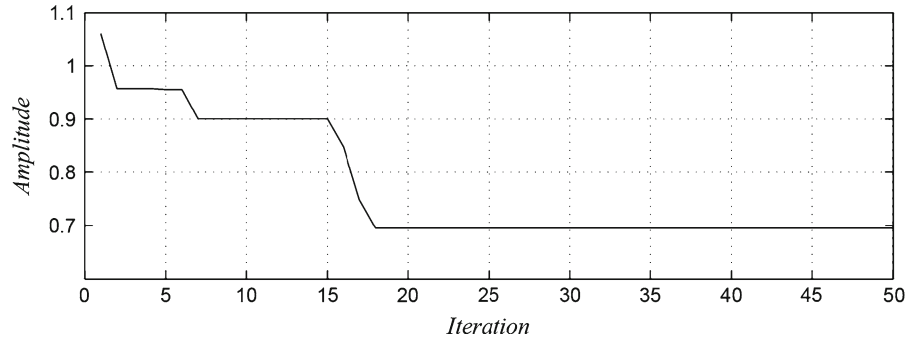


Fig. 4 Variations of the optimized parameters

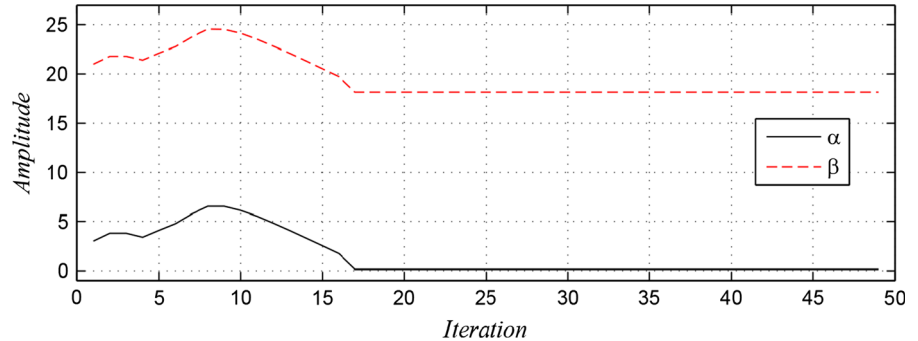
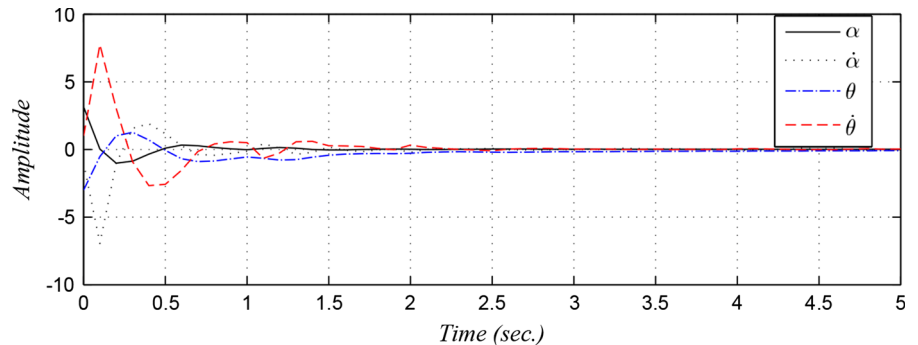


Fig. 5 The state trajectories



The nonlinear functions $\psi(\tilde{x}(t))$ and $\sigma(\tilde{x}(t))$ are defined in the form of (19) and (53), respectively, where the parameters α and β are obtained by solving the minimization problem (58) using the MRS method. Specifically, we begin the MRS algorithm with $\alpha = 2$ and $\beta = 20$. The MRS method gives the optimal parameters $\alpha = 0.126$, $\beta = 18.12$ after 17 number of iterations. Figures 3 and 4 demonstrate the variations of the cost function and the optimized parameters, respectively. The state trajectories of the system using the control law given in (59) are shown in Fig. 5. The trajectories of the system output and the tracking error are depicted in Fig. 6. It can be seen from Fig. 6 that the tracking error is regulated to zero by the proposed robust controller, irrespective of the time-varying delays and

uncertainties. Figure 7 demonstrates the control input which shows the good performance of the proposed method. The trajectory of the sliding curve is demonstrated in Fig. 8 where the sliding mode exists from the initial time $t = 0$.

When the state measurements are noise free, the control signal will be smooth because of the use of the boundary layer ε . Here, the effect of the measurement noise on the system states is considered. A zero-mean Gaussian measurement noise with standard deviation 0.01 is used which is shown in Fig. 9. When the state measurements are contaminated with uniform noise, the results are very similar to the results shown in Figs. 5, 6, 7 and 8. The trajectories of the tracking errors and control signal are illustrated in Figs. 10 and 11.

Fig. 6 **a** The system and reference model outputs, **b** the tracking error

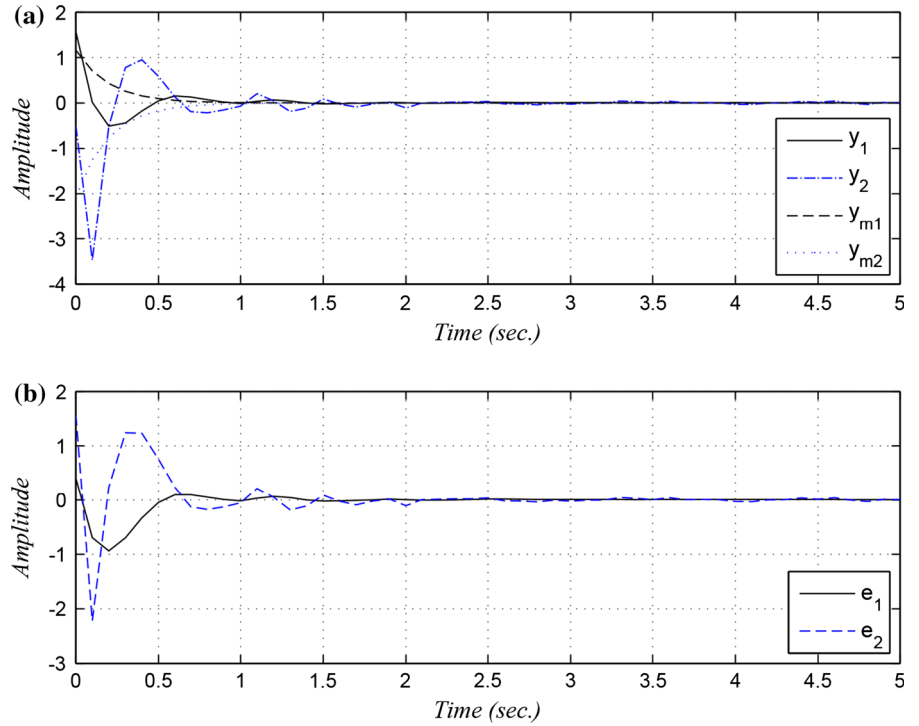


Fig. 7 The control signal

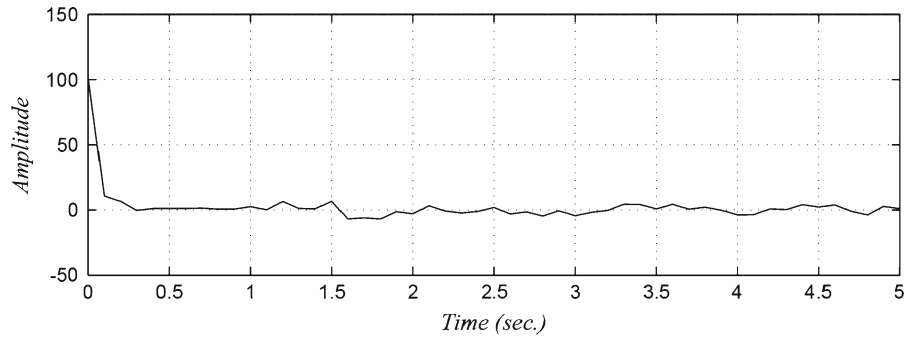
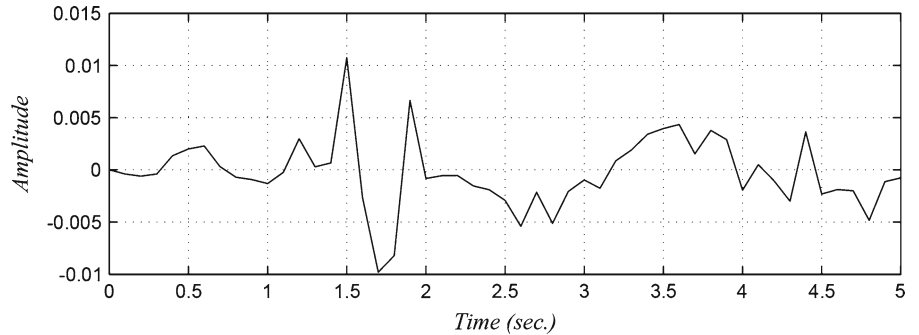


Fig. 8 The sliding curve



As it can be seen, the tracking errors and control signal have a slight chattering due to the measurement noise.

For robustness analysis, we select $\eta = 0.7$ and $L = [0.3 \ 0.8 \ 0.6 \ 0.5]$, and consider the initial conditions are set as: $x(0) = [0.8 \ 0.4 \ 0 \ 1.2]^T$,

Fig. 9 The measurement noise

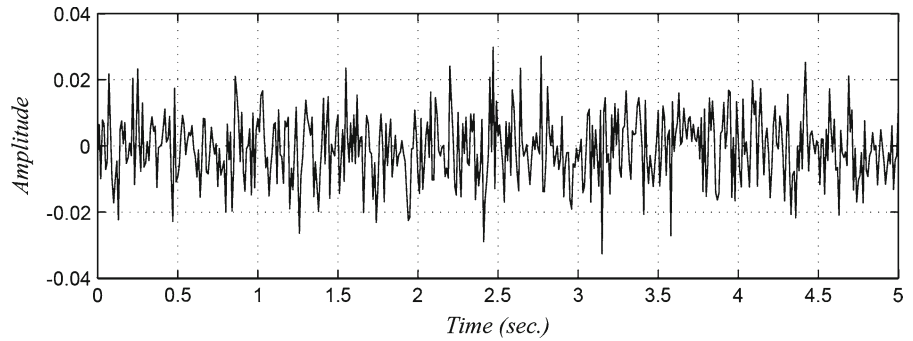


Fig. 10 The tracking errors

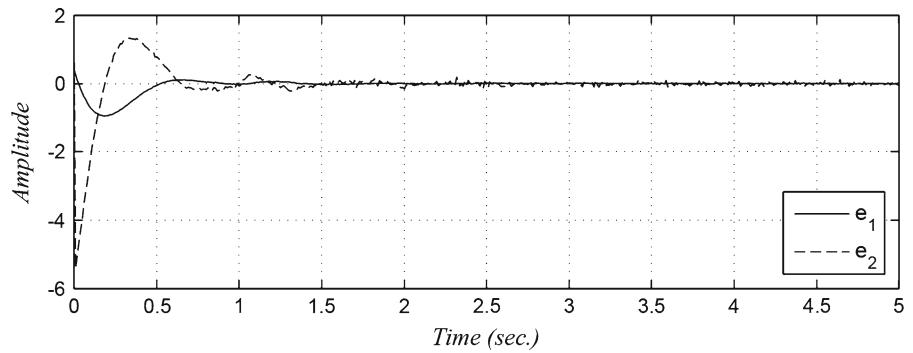
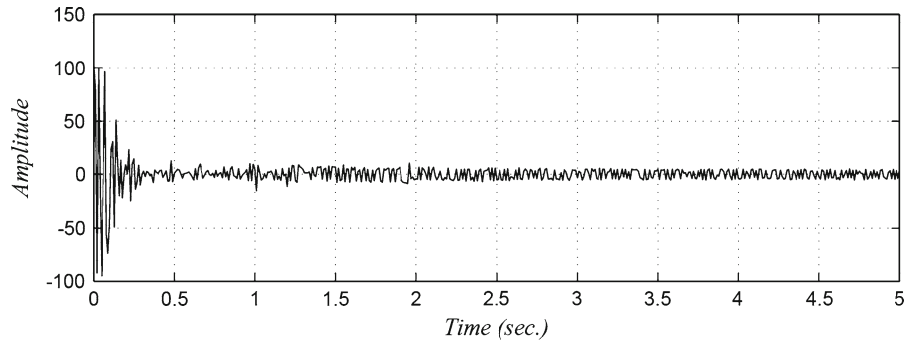


Fig. 11 The control signal



$x_m(0) = [1 \ 0.2 \ 0.4 \ 0.8]^T$. The uncertain time-varying parameters are selected as:

$$v(t) = 1 + 1.5 \sin(3t), \quad p(t) = 1.5 \cos(4t), \\ q(t) = 1.5 \cos(5t), \quad r(t) = 1.5 \cos(4t).$$

The trajectories of the system states, output, tracking error, control input and sliding curve are shown in Figs. 12, 13, 14 and 15, respectively. These results demonstrate the robustness of the proposed controller in the new conditions and show reasonable performance as well.

5.2 Example B: a vibrating uncertain time-delayed system

Consider the vibration of uncertain time-delayed system (1) which is proposed in [1] with:

$$A = \begin{bmatrix} 0 & 1 & 0 \\ 0 & 1 & 2 \\ -1 & -2 & 0 \end{bmatrix}, \quad B = \begin{bmatrix} 0 \\ 0.1 \\ 1 \end{bmatrix}, \\ C = [1 \ 1 \ 0], \quad N(r) = [r \ 0 \ 2r], \\ E(p) = p, \quad \tilde{W}(q) = q, \\ N_1 = 2, \quad N_{d1}(v) = [0 \ v \ 1.5v],$$

Fig. 12 The state trajectories

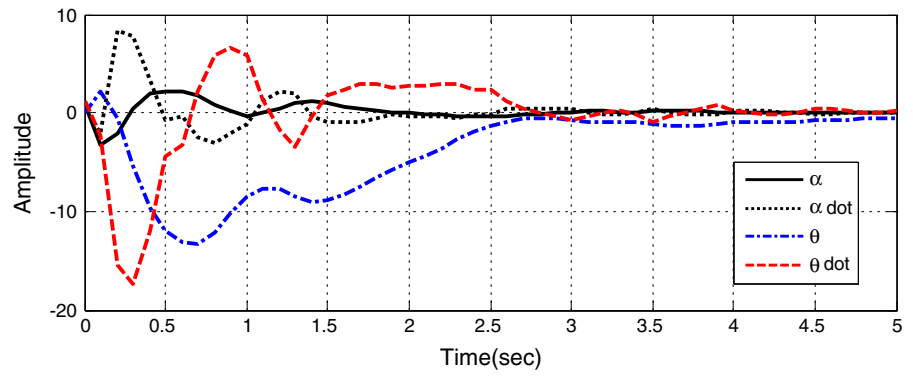


Fig. 13 a The system and reference model outputs, **b** the tracking error

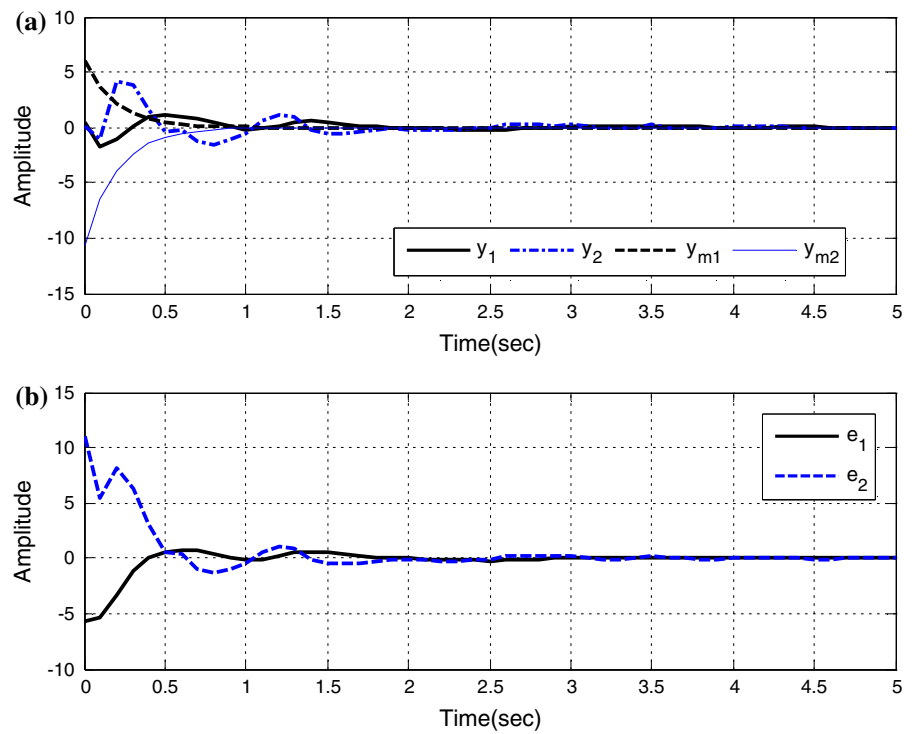


Fig. 14 The control signal

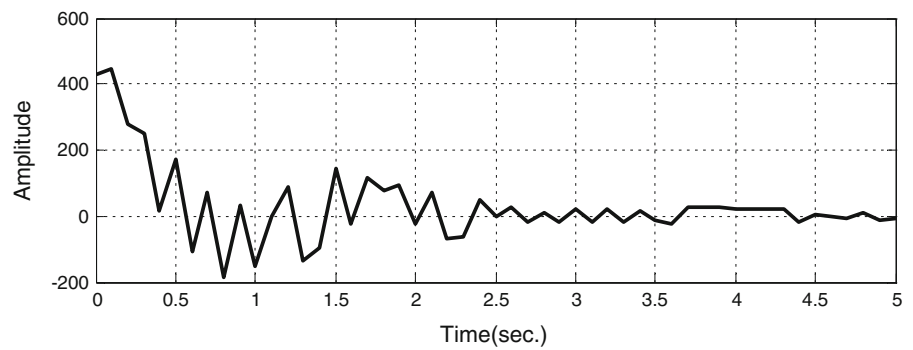
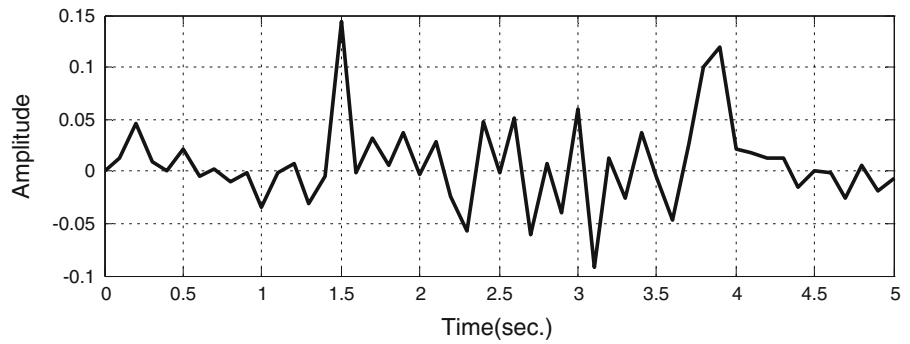


Fig. 15 The sliding curve



$$N_{d2}(v) = [v \ 2v \ 0], \quad \tau_1 = 1 + 0.5 \sin(\pi t),$$

$$\tau_2 = 1 - \cos(2t),$$

$$r = \sin(3t), \quad p = 1 - 0.5 \cos(2t),$$

$$q = 0.5 \sin(3t), \quad v = 1 + 0.5 \sin(2t).$$

The reference model with an oscillatory behavior is given by (2) with:

$$A_m = \begin{bmatrix} 0 & 1 \\ -1 & 0 \end{bmatrix}, \quad C_m = [1 \ 1]. \quad (67)$$

The constant parameters are selected as: $\eta = 0.3$, $\varepsilon = 0.3$, $\vartheta = 0.5$, and $L = [1 \ 0.5 \ 1]$. The initial conditions are given as: $x(0) = [0 \ 0 \ 0]^T$ and $x_m(0) = [1 \ 0]^T$. The open-loop system is unstable since its eigenvalues are: $\lambda_{1,2,3} = -0.433, 0.716 \pm j2.026$. Solving (3), the matrices G and H are obtained as:

$$G = \begin{bmatrix} 1 & 0 \\ 0 & 1 \\ -0.5786 & -0.5711 \end{bmatrix},$$

$$H = [1.5711 \ 1.4214].$$

Figures 16 and 17 show the trajectories of the tracking error and the desired and actual outputs, correspondingly. Also, the trajectories of the sliding surface and control input are displayed in Figs. 18 and 19, respectively. The simulation results confirm the stability of the closed-loop system subject to uncertainties and time-varying delays. The suggested technique can guarantee that the tracking error decreases asymptotically to zero.

5.3 Example C: an uncertain system with multiple time-varying delays

Extending the uncertain time-delay system given in [1, 34] to include multiple time-varying delays, we get:

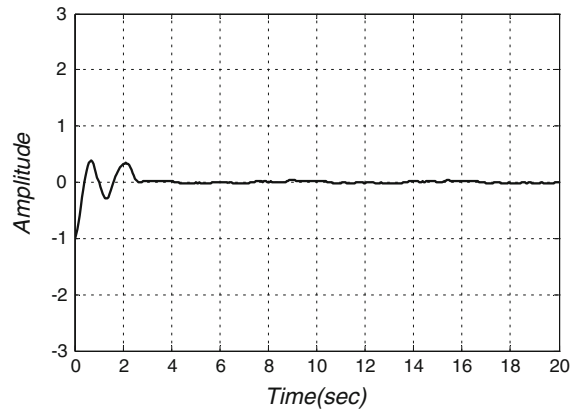


Fig. 16 The tracking error

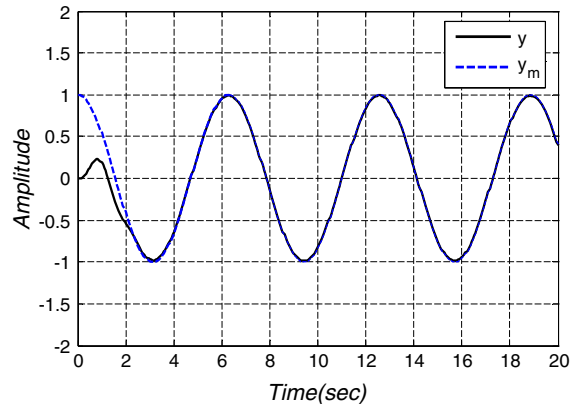


Fig. 17 Trajectories of the system and model outputs

$$\dot{x}(t) = \left(\begin{bmatrix} -1 & 1 \\ 0 & 2 \end{bmatrix} + \begin{bmatrix} 0 & 0 \\ r_1(t) & r_2(t) \end{bmatrix} \right) x(t)$$

$$+ \sum_{i=1}^3 \Delta A_{di}(v(t))x(t - \tau_i(t))$$

$$+ \left(\begin{bmatrix} 0 \\ 1 \end{bmatrix} + \begin{bmatrix} 0 \\ p(t) \end{bmatrix} \right) u(t) + \begin{bmatrix} 0 \\ 1 \end{bmatrix} q(t),$$

$$y = [1 \ 0] x(t), \quad (68)$$

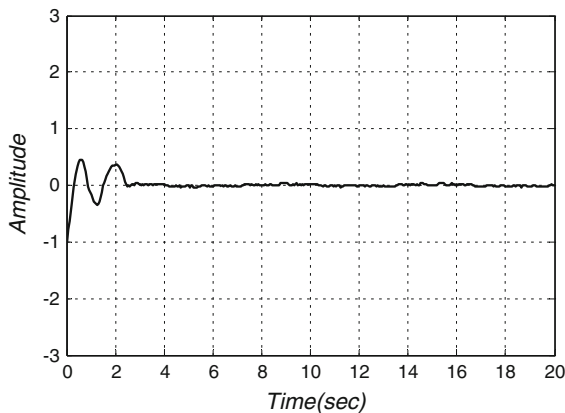


Fig. 18 The sliding surface

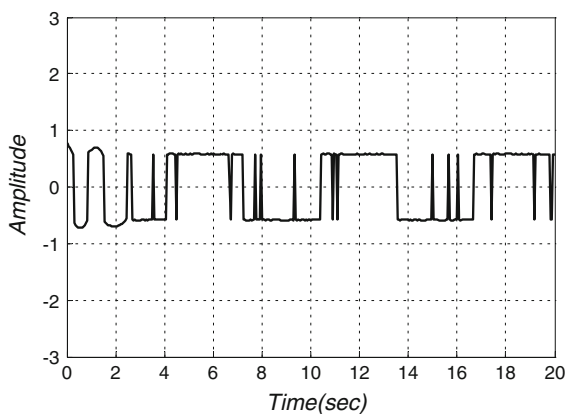


Fig. 19 Control input

where $\tau_i(t)$'s are time-delays. The disturbances and uncertainties have the following bounds:

$$|r_1(t)| \leq 0.5, \quad |r_2(t)| \leq 1, \quad |p(t)| \leq 0.5, \\ |q(t)| \leq 0.5, \quad |v(t)| \leq 1.5,$$

and

$$\Delta A_{d1}(v(t)) = \begin{bmatrix} 0 & 0 \\ 0 & v(t) \end{bmatrix}, \quad \Delta A_{d2}(v(t)) = \begin{bmatrix} 0 & 0 \\ v(t) & 0 \end{bmatrix}, \\ \Delta A_{d3}(v(t)) = \begin{bmatrix} 0 & 0 \\ v(t) & v(t) \end{bmatrix}.$$

The reference model is specified by:

$$\dot{x}_m(t) = \begin{bmatrix} -2 & 1 \\ 0 & -1 \end{bmatrix} x_m(t), \\ y_m(t) = [0 \ 1] x_m(t). \tag{69}$$

From (3), the solution of the matrices G and H can be obtained as follows:

$$G = \begin{bmatrix} 0 & 1 \\ 0 & 0 \end{bmatrix}, \quad H = [0 \ 0].$$

From (4) and (69), one can obtain: $N(r(t)) = [r_1(t) \ r_2(t)]$, $E(p(t)) = p(t)$, $\tilde{W}(q(t)) = q(t)$, $N_{d1}(v(t)) = [0 \ v(t)]$, $N_{d2}(v(t)) = [v(t) \ 0]$, $N_{d3}(v(t)) = [v(t) \ v(t)]$. Then, from (5), (18) and (69), the following parameters are calculated: $\rho_r = 1.12$, $\mu = 0.5$, $\rho_q = 0.5$, $\rho_{v1} = \rho_{v2} = 1.5$, $\rho_{v3} = 2.12$, $\|x_m(t)\| \leq M = 1.41$, $\rho = 9.3$. The constant parameters are selected as: $\alpha = 0.626$, $\beta = 6.01$, $L = [1 \ 1]$, $\eta = 0.3$, $\vartheta = 0.5$, and $\varepsilon = 0.2$. For the simulation purposes, the uncertain parameters $r_1(t)$, $r_2(t)$, $p(t)$, $q(t)$, $v(t)$, and initial conditions are set as follows:

$$r_1(t) = 0.5 \sin(3t), \quad r_2(t) = \sin(3t), \\ p(t) = 0.5 \cos(2t), \quad q(t) = 0.5 \sin(3t), \\ v(t) = 1 + 0.5 \sin(2t),$$

$x(0) = [3 \ 2]^T$, $x_m(0) = [1 \ 1]^T$. The time-varying delays $\tau_1(t)$, $\tau_2(t)$ and $\tau_3(t)$ are chosen as shown in Fig. 2, where $\tau_1(t) = \tau_3(t) = 1 + 0.5 \sin(\pi t)$.

The solution of the LMI is obtained using Matlab LMI toolbox which gives the following results:

$$P = \begin{bmatrix} 0.4011 & 0.3001 \\ 0.3001 & 0.6603 \end{bmatrix}, \quad K = [-1.5342 \ -3.2832], \\ S_1 = \begin{bmatrix} 2.7988 & -0.0580 \\ -0.0580 & 3.6189 \end{bmatrix}, \\ S_2 = \begin{bmatrix} 3.0058 & -0.1234 \\ -0.1234 & 3.6172 \end{bmatrix}, \\ S_3 = \begin{bmatrix} 2.8170 & 0.0008 \\ 0.0008 & 3.5605 \end{bmatrix}, \quad R_1 = \begin{bmatrix} 0.7622 & 1.0335 \\ 1.0335 & 1.8071 \end{bmatrix}, \\ R_2 = \begin{bmatrix} 0.7796 & 1.0348 \\ 1.0348 & 1.7991 \end{bmatrix}, \quad R_3 = \begin{bmatrix} 0.7741 & 1.0450 \\ 1.0450 & 1.8066 \end{bmatrix}.$$

The nonlinear function $\psi(\tilde{x}(t))$ is defined in the form of (19) and $\sigma(\tilde{x}(t))$ is in the form of (53). In the following, the simulation results of the proposed controller with the scaled nonlinear function are illustrated in comparison with the results of [1,34]. To compare the results with those of [1,34], the system is also simulated with the adaptive controllers given in [1,34]. Figure 20 shows the trajectories of the system states. This figure reveals the importance of adding the nonlinear function $\psi(\tilde{x}(t))$ for improving the system response. Figure 21 demonstrates the trajectory of the tracking errors and the error between the desired and actual outputs, respectively. As it can be seen from the results,

Fig. 20 The state trajectories

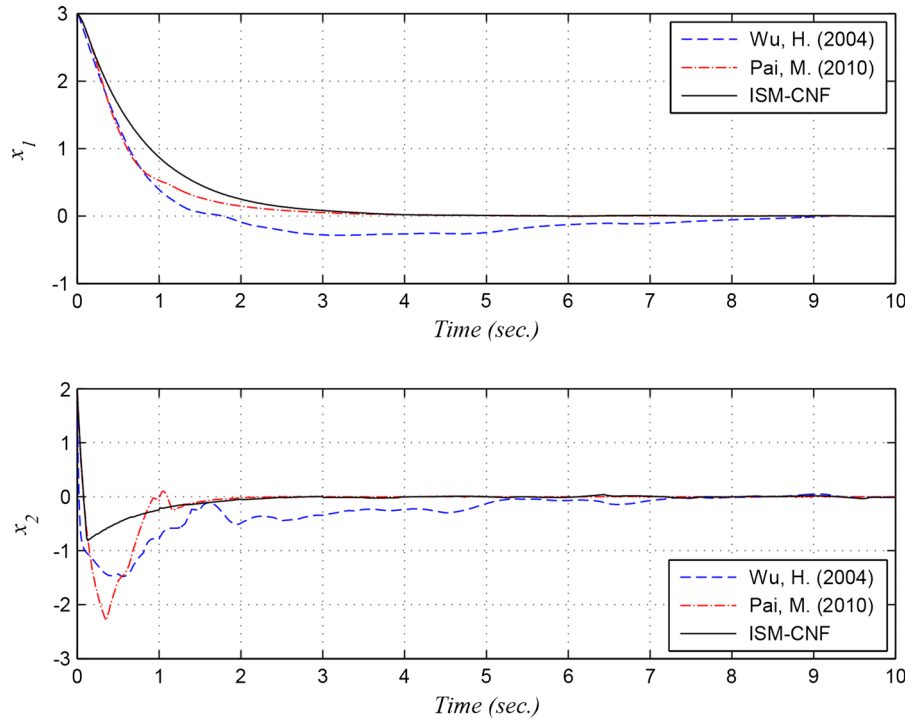
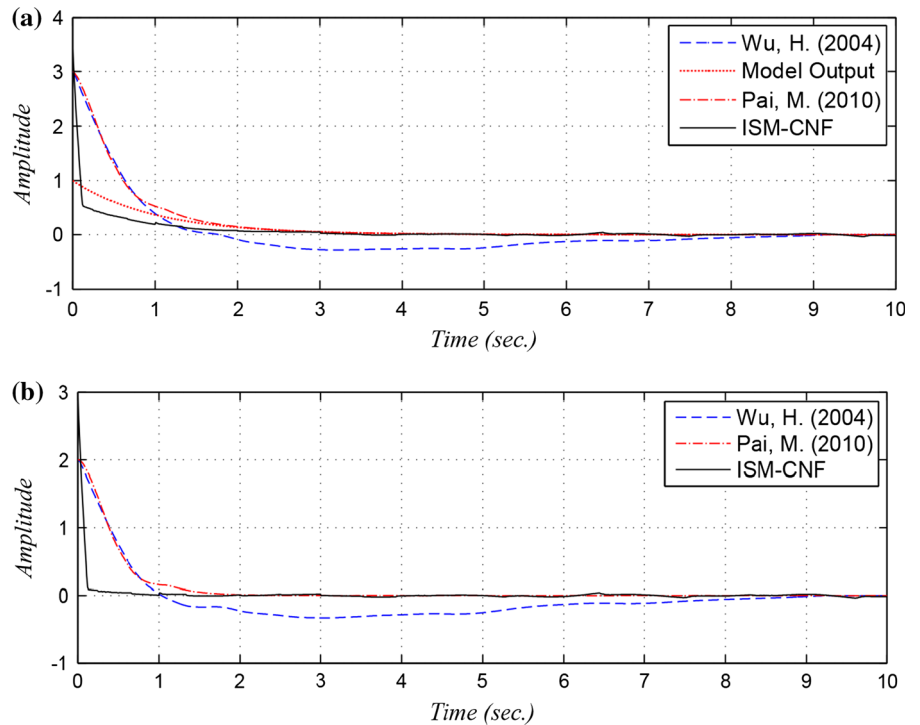


Fig. 21 **a** System output $y(t)$ and model output $y_m(t)$, **b** the tracking error $e(t)$



the proposed method provides faster and better transition responses over those of other methods. The trajectories of the sliding curves are illustrated in Fig. 22.

The comparison of the control inputs is illustrated in Fig. 23 which shows control signal of the proposed ISM-CNF method has much better behavior in compar-

Fig. 22 The sliding curves

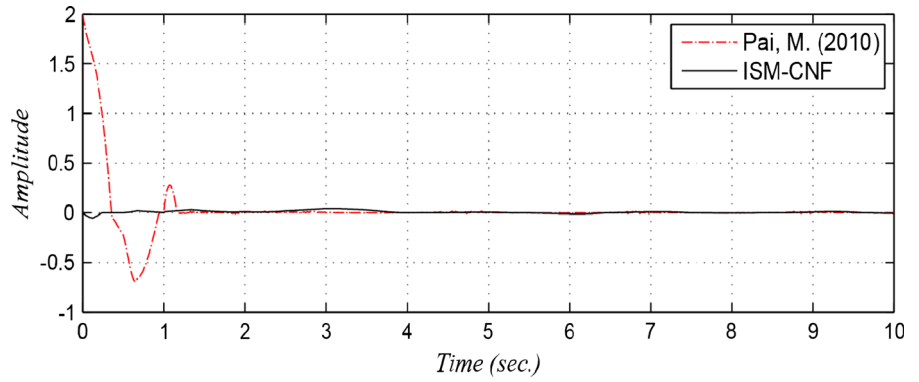


Fig. 23 The control signal

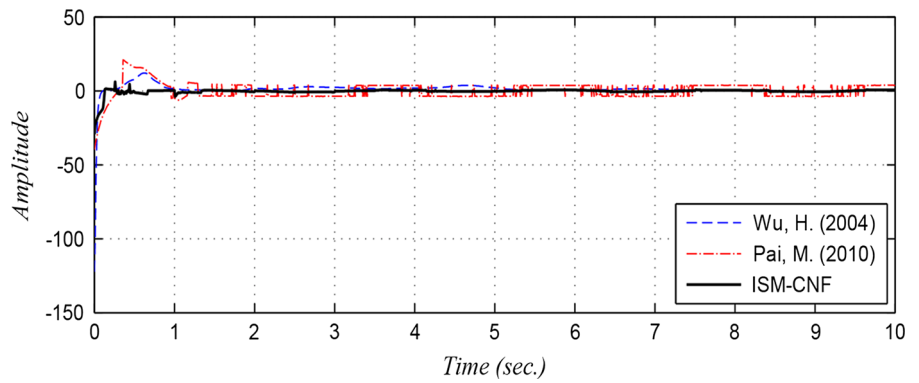
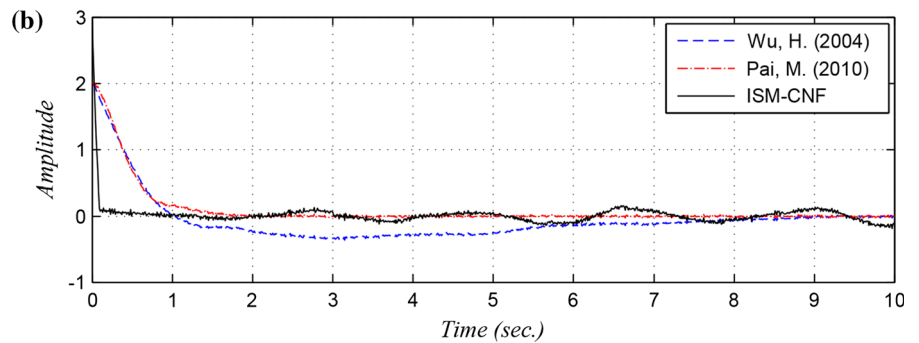
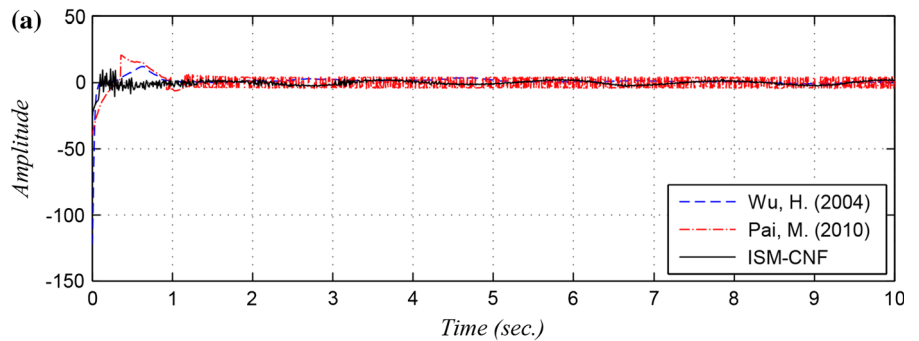


Fig. 24 **a** The control signal, **b** The tracking error with measurement noise



ison with those of the controllers in [1,34]. One can see that the control input proposed in this work approach

to the origin without any chattering. However, Fig. 23 shows that the control signal introduced in [1] contains

Table 1 IAE, ITAE and ISV of the system with ISM-CNF compared to those of [1,34]

	IAE	ITAE	ISV
Proposed ISM-CNF	0.315	0.248	34.532
Pai [1]	0.944	0.353	337.99
Wu [35]	2.294	6.233	363.93

high-frequency oscillations which are undesirable in practice. We repeat the simulation when the state measurements are contaminated by a zero-mean Gaussian noise with standard deviation 0.01. The trajectories of the tracking errors and control signal with measurement noise are illustrated in Fig. 24. The results are similar to the previous simulation, which demonstrates that the proposed method has good robust performance in the face of measurement noise, too.

The IAE, ITAE and ISV comparative results are given in Table 1. As it can be seen, the IAE, ITAE and ISV performance indices for tracking error and control signals are much smaller using the proposed ISM-CNF controller compared to other ones, which demonstrate the superior tracking improvement of the proposed method over the previous works. One can conclude from Table 1 that, for instance, the IAE improve-

ment of the tracking error and ISV improvement of the control input using ISM-CNF controller is three and 9.7 times better than those of [1], and 7.3 and 10.5 times better than those of [34], respectively.

To study the robustness of the proposed ISM-CNF controller and to compare its performance against those of the controllers of [1] and [34], the uncertain parameters $r_1(t)$, $r_2(t)$, $p(t)$, and $q(t)$ are changed with greater values as follow:

$$r_1(t) = 1.5 \sin(3t), \quad r_2(t) = 1.5 \sin(3t), \\ p(t) = \cos(2t), \quad q(t) = 5 \sin(3t).$$

Figure 25 shows the trajectories of the system states in the new conditions, with different magnitudes of disturbances and uncertainties. The trajectories of the system outputs and the sliding surfaces are illustrated in Fig. 26. The comparison of the control inputs and the tracking errors is shown in Fig. 27. It is seen that the proposed control input in this work is free of the chattering. In contrast, the control signal obtained by the sliding approach in [1] suffers of the chattering. All these figures verify that the proposed ISM-CNF method has much better robust performance in comparison with the controllers of [1,34].

For the new values of disturbances and uncertainties, the IAE, ITAE and ISV results are given in Table 2.

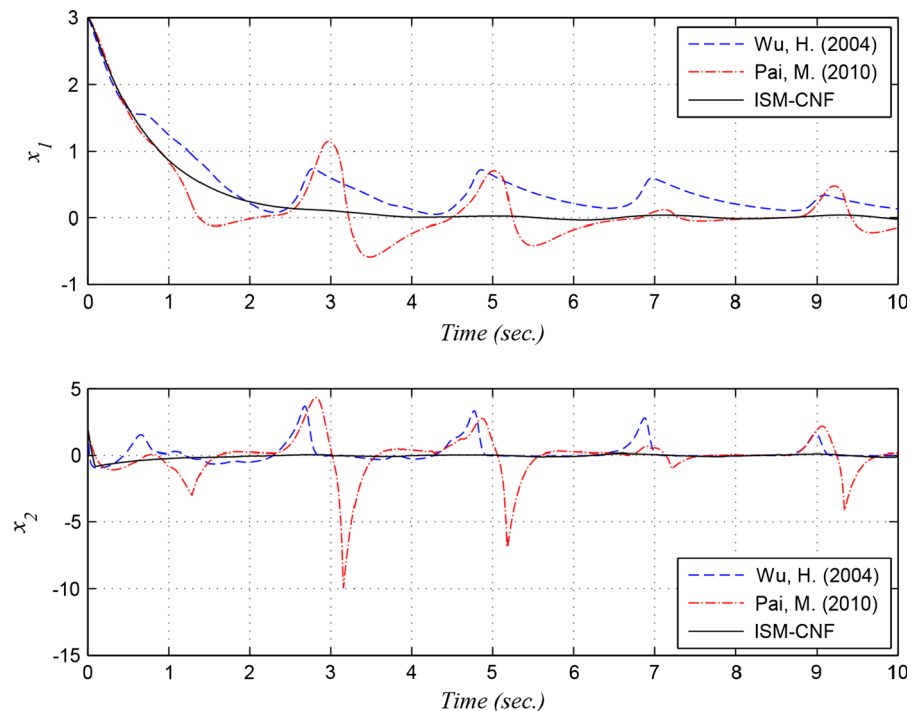
Fig. 25 The system states for greater values of disturbances and uncertainties

Fig. 26 **a** The system outputs, **b** the sliding curve

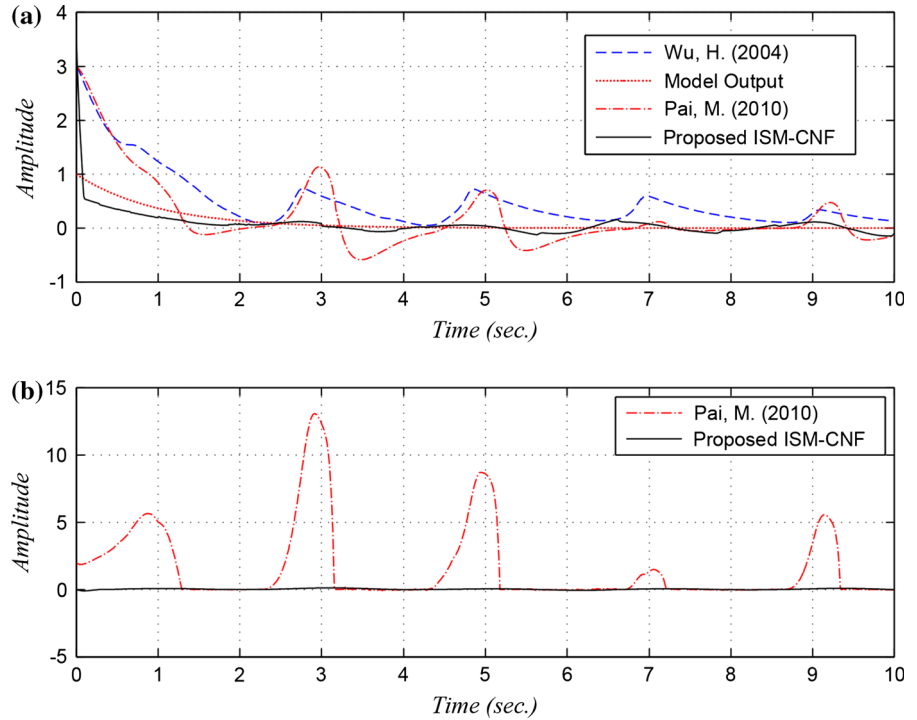
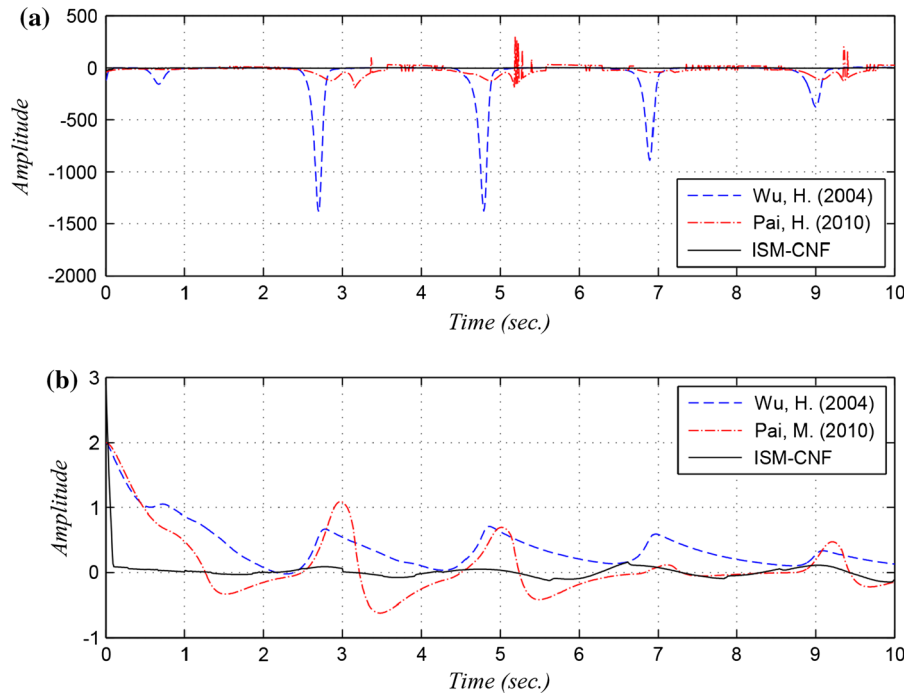


Fig. 27 **a** The control signal, **b** the tracking error



The IAE, ITAE and ISV performance indices are much less for the proposed ISM-CNF controller compared to other ones. For example, the IAE improvement of the tracking error and ISV improvement of the control

input using ISM-CNF controller is 4.7 and 14.3 times better than those of [1] and 5.8 and 17.8 times better than those of [34], respectively. Then, by comparing the results of Table 2, one can conclude that the tracking

Table 2 IAE, ITAE and ISV of the closed-loop system for greater values of disturbances and uncertainties

	IAE	ITAE	ISV
Proposed ISM-CNF	0.663	3.062	49.776
Pai [1]	3.162	9.746	711.07
Wu [35]	3.893	13.95	888.96

performance of the proposed ISM-CNF controller is superior to that of the controllers of [1] and [34].

6 Conclusions

In this paper, the theory of the combination of CNF and ISM techniques was considered for robust tracking and model following of linear MIMO systems with time-varying uncertain parameters, external disturbances and multiple delayed state perturbations. The ISM-CNF control law was designed to guarantee the tracking of the reference trajectory in the presence of uncertainties and without experiencing large overshoot, and keeping the invariance property of ISM method in rejecting disturbances. The asymptotic tracking conditions were provided in the form of an LMI. The resulting LMI was solved to obtain the controller gains as well as the Lyapunov–Krasovskii functional parameters. The effectiveness of the proposed method was shown by three simulation examples. As it can be observed from the simulation results, the state trajectories are successfully regulated to zero in the face of measurement noise and chattering effects, and the proposed method yields much better robust performance in comparison with the results of the controllers of [1, 34]. The design method can be considered as a promising way for controlling similar nonlinear systems.

References

- Pai, M.C.: Design of adaptive sliding mode controller for robust tracking and model following. *J. Franklin Inst.* **347**, 1837–1849 (2010)
- Chang, J.L.: Dynamic output feedback sliding mode control for uncertain mechanical systems without velocity measurements. *ISA Trans.* **49**, 229–234 (2010)
- Aghababa, M.P.: No-chatter variable structure control for fractional nonlinear complex systems. *Nonlinear Dyn.* **73**, 2329–2342 (2013)
- Mobayen, S.: Design of LMI-based global sliding mode controller for uncertain nonlinear systems with application to Genesio's chaotic system. *Complexity* (2014). doi:[10.1002/cplx.21545](https://doi.org/10.1002/cplx.21545)
- Mobayen, S., Yazdanpanah, M.J., Majd, V.J.: A finite-time tracker for nonholonomic systems using recursive singularity-free FTSM. In: 2011 American control Conference, San Francisco, CA, USA, pp. 1720–1725 (2011)
- Mobayen, S.: Finite-time robust-tracking and model-following controller for uncertain dynamical systems. *J. Vib. Control* (2014). doi:[10.1177/1077546314538991](https://doi.org/10.1177/1077546314538991)
- Mobayen, S.: Fast terminal sliding mode controller design for nonlinear second-order systems with time-varying uncertainties. *Complexity* (2014). doi:[10.1002/cplx.21600](https://doi.org/10.1002/cplx.21600)
- Hamayun, M., Edwards, C., Alwi, H.: Design and analysis of an integral sliding mode fault-tolerant control scheme. *IEEE Trans. Autom. Control* **57**, 1783–1789 (2012)
- Pai, M.C.: Discrete-time output feedback quasi-sliding mode control for robust tracking and model following of uncertain systems. *J. Franklin Inst.* **351**, 2623–2639 (2014)
- Aghababa, M.P.: Synchronization and stabilization of fractional second order nonlinear complex systems. *Nonlinear Dyn.* (2014). doi:[10.1007/s11071-014-1411-4](https://doi.org/10.1007/s11071-014-1411-4)
- Faieghi, M.R., Kuntanapreeda, S., Delavari, H., Baleanu, D.: LMI-based stabilization of a class of fractional-order chaotic systems. *Nonlinear Dyn.* **72**, 301–309 (2013)
- Mobayen, S.: An LMI-based robust controller design using global nonlinear sliding surfaces and application to chaotic systems. *Nonlinear Dyn.* (2014). doi:[10.1007/s11071-014-1724-3](https://doi.org/10.1007/s11071-014-1724-3)
- Gao, Q., Liu, L., Feng, G., Wang, Y., Qiu, J.: Universal fuzzy integral sliding-mode controllers based on T-S fuzzy models. *IEEE Trans. Fuzzy Syst.* **22**, 350–352 (2014)
- Zheng, Z., Sun, W., Chen, H., Yeow, J.T.W.: Integral sliding mode based optimal composite nonlinear feedback control for a class of systems. *Control Theory Technol.* **12**, 139–146 (2014)
- Gao, Z., Liao, X.: Integral sliding mode control for fractional-order systems with mismatched uncertainties. *Nonlinear Dyn.* **72**, 27–35 (2013)
- Chang, J.L.: Dynamic output feedback integral sliding mode control design for uncertain systems. *Int. J. Robust Nonlinear Control* **22**, 841–857 (2012)
- Ting, H.C., Chang, J.L., Chen, Y.P.: Output feedback integral sliding mode controller of time-delay systems with mismatch disturbances. *Asian J. Control* **14**, 85–94 (2012)
- Sun, H., Li, S., Sun, C.: Finite time integral sliding mode control of hypersonic vehicles. *Nonlinear Dyn.* **73**, 229–244 (2013)
- Zhao, L.W., Hua, C.C.: Finite-time consensus tracking of second-order multi-agent systems via nonsingular TSM. *Nonlinear Dyn.* **75**, 311–318 (2014)
- Fei, J., Ding, H.: Adaptive sliding mode control of dynamic system using RBF neural network. *Nonlinear Dyn.* **70**, 1563–1573 (2012)
- Wang, L., Sheng, Y., Liu, X.: A novel adaptive high-order sliding mode control based on integral sliding mode. *Int. J. Control Autom. Syst.* **12**, 459–472 (2014)
- Mondal, S., Mahanta, C.: Composite nonlinear feedback based discrete integral sliding mode controller for uncer-

- tain systems. *Commun. Nonlinear Sci. Numer. Simul.* **17**, 1320–1331 (2011)
23. Mobayen, S.: Robust tracking controller for multivariable delayed systems with input saturation via composite nonlinear feedback. *Nonlinear Dyn.* **76**, 827–838 (2014)
 24. Mobayen, S., Majd, V.J.: Robust tracking control method based on composite nonlinear feedback technique for linear systems with time-varying uncertain parameters and disturbances. *Nonlinear Dyn.* **70**, 171–180 (2012)
 25. Mobayen, S.: Design of CNF-based nonlinear integral sliding surface for matched uncertain linear systems with multiple state-delays. *Nonlinear Dyn.* **77**, 1047–1054 (2014)
 26. Cheng, G., Peng, K.: Robust composite nonlinear feedback control with application to a servo positioning system. *IEEE Trans. Ind. Electron.* **54**, 1132–1140 (2007)
 27. Lan, W., Thum, C.K., Chen, B.M.: A hard-disk-drive servo system design using composite nonlinear feedback control with optimal nonlinear gain tuning methods. *IEEE Trans. Ind. Electron.* **57**, 1735–1745 (2010)
 28. Peng, K., Chen, B.M., Cheng, G., Lee, T.H.: Modeling and compensation of nonlinearities and friction in a micro hard disk drive servo system with nonlinear feedback control. *IEEE Trans. Control Syst. Technol.* **13**, 708–721 (2005)
 29. Mondal, S., Mahanta, C.: A fast converging robust controller using adaptive second order sliding mode. *ISA Trans.* **51**, 713–721 (2012)
 30. Bandyopadhyay, B., Deepak, F., Park, Y.J.: A robust algorithm against actuator saturation using integral sliding mode and composite nonlinear feedback. In: *Proceedings of the 17th World Congress, The International Federation of Automatic Control, COEX, South Korea*, pp. 14174–14179 (2008)
 31. Mobayen, S.: Finite-time stabilization of a class of chaotic systems with matched and unmatched uncertainties: an LMI approach. *Complexity* (2014). doi:[10.1002/cplx.21624](https://doi.org/10.1002/cplx.21624)
 32. Mobayen, S., Majd, V.J., Sojoodi, S.: An LMI-based composite nonlinear feedback terminal sliding-mode controller design for disturbed MIMO systems. *Math. Comput. Simul.* **85**, 1–10 (2012)
 33. Pai, M.C.: Discrete-time sliding mode control for robust tracking and model following of systems with state and input delays. *Nonlinear Dyn.* **76**, 1769–1779 (2014)
 34. Wu, H.: Adaptive robust tracking and model following of uncertain dynamical systems with multiple time delays. *IEEE Trans. Autom. Control* **49**, 611–616 (2004)
 35. Wu, H.: Adaptive robust control of uncertain dynamical systems with multiple time-varying delays. *IET Control Theory Appl.* **4**, 1775–1784 (2010)
 36. Pai, M.C.: Robust tracking and model following of uncertain dynamic systems via discrete-time integral sliding mode control. *Int. J. Control Autom. Syst.* **7**, 381–387 (2009)
 37. Hespanha, J.P.: *Linear Systems Theory*. Princeton University Press, Princeton (2009)
 38. Chesi, G.: LMI techniques for optimization over polynomials in control: a survey. *IEEE Trans. Autom. Control* **55**, 2500–2510 (2010)
 39. Li, T.H.S., Huang, Y.C.: MIMO adaptive fuzzy terminal sliding-mode controller for robotic manipulators. *Inf. Sci.* **180**, 4641–4660 (2010)
 40. Hassanzadeh, I., Mobayen, S.: Controller design for rotary inverted pendulum system using evolutionary algorithms. *Math. Probl. Eng.* **2011**, 1–17 (2011)
 41. Zhang, J., Xia, Y.: Design of static output feedback sliding mode control for uncertain linear systems. *IEEE Trans. Ind. Electron.* **57**, 2061–2070 (2010)
 42. Bandyopadhyay, B., Deepak, F., Kim, K.S.: *Sliding Mode Control Using Novel Sliding Surfaces*. Springer, Berlin Heidelberg (2009)
 43. Delavari, H., Ranjbar, A.N., Ghaderi, R.: Fractional order control of a coupled tank. *Nonlinear Dyn.* **61**, 383–397 (2010)
 44. Lim, C.W., Park, Y.J., Moon, S.J.: Robust saturation controller for linear time-invariant system with structured real parameter uncertainties. *J. Sound Vib.* **294**, 1–14 (2006)
 45. Lingrong, D., Zhixiang, T.: First order dynamic sliding mode control for wheeled mobile robots. *Commun. Comput. Inf. Sci.* **232**, 373–381 (2011)
 46. Falahpoor, M., Ataei, M., Kiyoumars, A.: A chattering-free sliding mode control design for uncertain chaotic systems. *Chaos Soliton Fractals* **42**, 1755–1765 (2009)
 47. Hassanzadeh, I., Harifi, A., Arvani, F.: Design and implementation of an adaptive control for a robot. *Am. J. Appl. Sci.* **4**, 56–59 (2007)
 48. Hassanzadeh, I., Mobayen, S.: PSO-based controller design for rotary inverted pendulum system. *J. Appl. Sci.* **8**, 2907–2912 (2008)